

DESIGN AND DEVELOPMENT OF LATEX CUPS  
COLLECTOR ROBOT V3  
(MECHANICAL)

KHOR PEY WEN

UNIVERSITI TUNKU ABDUL RAHMAN

DESIGN AND DEVELOPMENT OF LATEX CUPS ROBOT COLLECTOR V3  
(MECHANICAL)

KHOR PEY WEN

A project report submitted in partial fulfilment of the  
requirements for the award of the degree of  
Bachelor of Engineering (Honours) Industrial Engineering

Faculty of Engineering and Green Technology  
Universiti Tunku Abdul Rahman

May 2023

## DECLARATION

I hereby declare that this project report is based on my original work except for citations and quotations which have been duly acknowledged. I also declare that it has not been previously and concurrently submitted for any other degree or award at UTAR or other institutions

Signature :

A handwritten signature in black ink, appearing to read 'Khor Pey Wen', is written over a light blue grid background.

Name : KHOR PEY WEN

ID No. : 18AGB03828

Date : 21/4/2023

## APPROVAL FOR SUBMISSION

I certify that this project report entitled “DESIGN AND DEVELOPMENT OF LATEX CUPS COLLECTOR ROBOT V3 (MECHANICAL)” was prepared by KHOR PEY WEN has met the required standard for submission in partial fulfilment of the requirements for the award of Bachelor of Engineering (Hons) Industrial Engineering at Universiti Tunku Abdul Rahman.

Approved by,

Signature :  \_\_\_\_\_

Supervisor : Dr. Lim Chong Hooi

Date : 24/4/2023

Signature :  \_\_\_\_\_

CO-Supervisor: Ts. Tan Yee Chyan

Date : 24/4/2023

The copyright of this report belongs to the author under the terms of the copyright Act 1987 as qualified by Intellectual Property Policy of Universiti Tunku Abdul Rahman. Due acknowledgement shall always be made of the use of any material contained in, or derived from, this report.

© Year, Name of candidate. All right reserved.

Specially dedicated to  
my beloved grandmother, mother and father

## ACKNOWLEDGEMENTS

I would like to thank everyone who had contributed to the successful completion of this project. I would like to express my gratitude to my research supervisor, Dr. Lim Chong Hooi for his invaluable advice, guidance and his enormous patience throughout the development of the research.

In addition, I would also like to express my gratitude to my loving parent and friends who had helped and given me support and encouragement.

DESIGN AND DEVELOPMENT OF LATEX CUPS COLLECTOR ROBOT V3  
(MECHANICAL)

**ABSTRACT**

Rubber is widely used in the production of products such as gloves, tyres, and mattresses, and the demand for rubber products is increasing over time. Nonetheless, global rubber production has declined in recent years due to a variety of factors, including both environmental and human factors. The lack of manpower in latex collection is one of the main reasons for the reduction in rubber production. This project developed an automated robot prototype that collects latex cups in order to improve global rubber production by assisting workers in rubber plantations. The robot was designed on a mobile platform equipped with a motor-driven Five Degree of Freedom (DoF) manipulator arm, Ackermann steering, double wishbone suspension, rear-wheel drive and a latex storage tank to store the latex collected from the trees. The robot was equipped with ultrasonic sensors to locate latex cups and rubber trees so that it could move and perform tasks accurately. In addition, encoder sensor modules were used to improve the accuracy of the movements by measuring the rotational speed of the motors. The yield strength of the PLA plastic material used in developing the latex cup collector robot is  $7.00 \times 10^7 \text{N/m}^2$  and the maximum stress of the critical parts should not exceed the maximum yield strength of the PLA plastic. The robot prototype has gone through tests such as a mobility test, a static test and a balance test to test its functionality and stability. The height of the barrier used to conduct mobility test is 10mm and 15mm. Other than that, the robot prototype has also performed test runs to validate its control system. These findings demonstrated that the prototype design is workable and capable of carrying out fundamental duties automatically on the uneven terrain of the rubber plantation.

## TABLE OF CONTENTS

<b>DECLARATION</b>	<b>iii</b>
<b>APPROVAL FOR SUBMISSION</b>	<b>iv</b>
<b>ACKNOWLEDGEMENTS</b>	<b>vii</b>
<b>ABSTRACT</b>	<b>viii</b>
<b>LIST OF TABLES</b>	<b>xiii</b>
<b>LIST OF FIGURES</b>	<b>xiv</b>
<b>LIST OF SYMBOLS/ ABBREVIATIONS</b>	<b>xviii</b>
<b>CHAPTER 1</b>	<b>1</b>
<b>INTRODUCTION</b>	<b>1</b>
1.1 Background	1
1.2 Problem Statements	3
1.3 Aims and Objectives	5
1.4 Scope of Project	5
<b>CHAPTER 2</b>	<b>6</b>
<b>LITERATURE REVIEW</b>	<b>6</b>
2.1 Latex	6
2.2 Automated Agricultural Harvesting	7
2.3 Obstacles in Deploying Agricultural Robot	8
2.4 Components of Agricultural Robot	9
2.4.1 Mobility and Steering	10
2.4.1.1 Transmission	10

2.4.1.2 Locomotion	11
2.4.1.3 Steering	13
2.4.1.4 Suspension	15
2.4.2 Manipulation	17
2.4.2.1 Manipulator	18
2.4.2.2 End-Effector	19
2.4.3 Sensing	19
2.4.4 Path Planning	20
2.5 Improvement from Previous Research	20
<b>CHAPTER 3</b>	<b>21</b>
<b>METHODOLOGY</b>	<b>21</b>
3.1 Chosen Design	21
3.2 Design of Robot Prototype and Choice of Material	21
3.2.1 Properties of PLA Plastic Material in Solidworks	22
3.2.2 Transmission System Design (Differential)	23
3.2.3 Locomotion System Design (Wheels)	24
3.2.4 Suspension System Design (Double wishbone and spring)	25
3.2.5 Steering System Design (Ackermann Mechanism)	28
3.2.6 Manipulator Design	30
3.2.7 End effector Design (Gripper)	34
3.2.8 Storage Tank Design	36
3.2.9 Encoder sensor holder	38
3.2.10 Electronic components holder	39
3.2.11 Base Storage Compartment	40
3.2.12 Solidworks Assembly	40
3.2.12.1 Mobility components	40
3.2.12.2 Manipulation components	41
3.2.12.3 Overall Assembly	42
3.3 Firmware configuration	42
3.3.1 Parameter calculation	44

3.3.1.1 Motor for robot transmission	44
3.3.1.2 Motor for robotic arm	47
3.3.1.3 Motor for gripper rotation (Pouring)	48
3.4 Static Analysis	50
3.4.1 Robot Platform	50
3.4.2 Robotic Arm	54
3.5 Centre of mass: Toppling analysis	55
3.5.1 Centre of mass identification	55
3.5.2 Topple Angle	57
3.6 Motion Study	58
3.6.1 Motor Feature	59
3.6.2 Spring Feature	60
3.6.3 Contact Feature	60
3.7 Fabrication of Prototype and Experiment Setup	61
3.7.1 Fabrication of Prototype	61
3.7.2 Experiment Setup	61
3.7.2.1 Setup for Topple Angle Test	62
3.7.2.2 Setup for Prototype Test Run	62
3.8 Project Planning and Milestone	64
<b>CHAPTER 4</b>	<b>68</b>
<b>RESULTS AND DISCUSSIONS</b>	<b>68</b>
4.1 Latex Cup Collector Robot Prototype	68
4.2 Finite Element Analysis (Static test)	69
4.2.1 Robot Platform	70
4.2.2 Robotic Arm	72
4.3 Centre of mass: Toppling Analysis	74
4.3.1 Centre of mass	74
4.3.2 Topple Angle	76
4.4 Prototype test run	77
4.4.1 Functional test	77
4.4.2 Manipulator test	79
4.5 Mobility Test	80

4.5.1 Motion Study	81
4.5.2 Mobility Test Run	83
4.6 Comparison with Previous Versions of Robot Prototype	84
<b>CHAPTER 5</b>	<b>86</b>
<b>CONCLUSION AND RECOMMENDATIONS</b>	<b>86</b>
5.1 Conclusion	86
5.2 Recommendations	86
<b>REFERENCES</b>	<b>88</b>

## LIST OF TABLES

<b>TABLE</b>	<b>TITLE</b>	<b>PAGE</b>
3.1	Selected mechanisms for each design sub-function	21
3.2	Firmware configuration and specification	43
3.3	Forces exerted on the robot platform	51
3.4	Weight of each components of robotic arm	52
3.5	Eight centre of mass identification situations	56
3.6	Gantt chart of FYP1	66
3.7	Gantt chart of FYP2	67
4.1	Centre of mass of robot prototype for eight situations	75
4.2	Theoretical topple angle for eight scenarios	76
4.3	Theoretical and Experimental topple angle and percentage errors	76
4.4	Steps and cycle time	78
4.5	Comparison of Previous Versions of Robot Prototype with Current Version	84

## LIST OF FIGURES

<b>FIGURE</b>	<b>TITLE</b>	<b>PAGE</b>
1.1	Rubber Production in Malaysia from year 2017 to 2021 (in thousand tonnes) (Source: MRC, 2021)	3
1.2	Rubber Consumption in Malaysia from year 2017 to 2021 (in thousand tonnes) (Source: MRC, 2021)	4
2.1	Rubber tree latex (Source: Liné, 2020)	7
2.2	Structure of task sub-systems in an agricultural robot (Source: Bechar, 2016)	9
2.3	Example of leg locomotion system (Source: Tedeschi, 2014)	12
2.4	RT Mover (source: Nakajima, 2011)	13
2.5	Ackermann steering principle (Hrbacek., n.d.)	14
2.6	Rocker-bogie suspension system (Source: Technology Robotix Society, 2019)	17
3.1	Properties of PLA plastic material in Solidworks	22
3.2	Differential gear model in Solidworks	23
3.3	Differential gear box in Solidworks	24
3.4	Differential gear transmission in Solidworks	24
3.5	Front wheel design	25
3.6	Rear wheel design	25
3.7	Uncompressed and compressed conditions of shock absorber	26

3.8	Front wheel system: Double wishbone suspension system (a) When both sides are at their initial position; (b) While one of the shock absorbers is compressed	27
3.9	Spring suspension system used in the rear wheel	27
3.10	Extended arm on wheel hub	28
3.11	Design of ball joint	28
3.12	Connection between steering bar and wheel hubs using ball joint linkage rods	29
3.13	Wheels are aligned straight and the gear was set at default position	29
3.14	Both wheels turn left when the servo motor rotates its shaft anti-clockwise	30
3.15	Both wheels turn right when the servo motor rotates its shaft clockwise	30
3.16	EEZYbotARM MK2 (Source: Carlo, 2018)	31
3.17	Front view of manipulator base design for horizontal movement	32
3.18	Main arm of manipulator system design	33
3.19	Manipulator horizontal arm design	33
3.20	Gripper support design	34
3.21	Gripper end-effector design	35
3.22	Motor holder design	35
3.23	Gripper holder design	35
3.24	Gear mechanism that drives the gripper rotation	36
3.25	Storage tank, pipe and funnel design	36
3.26	Fitting of storage tank into the robot platform's slots	37
3.27	Reinforcing design at bottom of the robot platform	38
3.28	Encoder sensor holder for base with horizontal movement	38

3.29	Electronic components holder with slot	39
3.30	Electronic components holder with double layer	39
3.31	Base storage compartment for DC motor	40
3.32	Mobility subsystem (Isometric view)	41
3.33	Assembly of manipulation components	41
3.34	The latex cup robot collector's overall prototype design	42
3.35	A free-body diagram of robot on an inclined terrain with slope $\theta$	44
3.36	Forces exerted perpendicular to point O of the main arm	47
3.37	3 separated parts of gripper set	48
3.38	Position of components on the robot platform (top & bottom)	51
3.39	Simplified free body diagram of extended robotic arm	52
3.40	Fixture set on the robot platform	54
3.41	Static analysis of robotic arm Solidworks	54
3.42	Left and back topple free body diagram	58
3.43	Uneven terrain created for Motion Study in Solidworks	59
3.44	Motor feature setting in Solidworks	59
3.45	Spring feature of front wheel system in Solidworks	60
3.46	Spring feature of rear wheel system in Solidworks	60
3.47	Laptop stand with adjustable height for topple angle testing	62
3.48	Rubber trees setup	63
3.49	Latex cups positioned at different heights	63
3.50	Barriers arrangement for mobility test	63
3.51	The project's overall flowchart	64

4.1	Latex Cup Collector Robot Prototype (Isometric View)	68
4.2	Latex Cup Collector Robot Prototype (front, rear, right and left view)	69
4.3	Stress plot for robot platform	70
4.4	Displacement plot of robot platform	71
4.5	Strain plot of robot platform	71
4.6	Stress plot of extended robotic arm	72
4.7	Stress plot of the gripper part (Section view)	73
4.8	Displacement plot of extended robotic arm	73
4.9	Strain plot of extended robotic arm	74
4.10	Measurement of centre of mass in x, y and z direction	75
4.11	Procedure of the prototype to collect latex cup for single cycle	78
4.12	Robot collects latex cup positioned at 190 mm height	80
4.13	Robot collects latex cup positioned at 150 mm height	80
4.14	Robot collects latex cup positioned at 90 mm height	80
4.15	Yaw, pitch and roll of the robot prototype	81
4.16	Motion study: Yaw, Pitch, and Roll angle ( $^{\circ}$ ) vs. time (s) graph	82
4.17	Side view of robot prototype travel across left and right barriers	83
4.18	Front view of robot prototype travel across left and right barriers	84

## LIST OF SYMBOLS/ ABBREVIATIONS

$a$	acceleration of robot, $m/s^2$
$d_n$	Distance between $F_n$ and point O, where $n = A$ and $B$ , mm
$F_n$	Force exerted perpendicular to the point O, where $n = A$ and $B$ , N
$F_s$	weight of loads, N
$F_y$	forces acting at the Y direction, N
$f_{wheel}$	the force pushing against the wheel, N
$f_{gravity}$	force pulling robot down incline due to gravity, N
$g$	gravity, $m/s^2$
$H_{it}$	height of inner tank, mm
$I_{part\ 1\ \&\ 2}$	mass moment of inertia of part 1 and 2, $kg \cdot m^2$
$I_{part\ 3}$	mass moment of inertia of part 3, $kg \cdot m^2$
$k$	spring constant, N/mm
$L_0$	Initial spring length, mm
$L_c$	Compressed spring length, mm
$L_{it}$	length of inner tank, mm
$M_A$	moment at point A, $N \cdot mm$
$m_c$	mass of component, kg
$m_n$	mass of parts, g
$m_{robot}$	mass of the robot, kg
$RPM_{input}$	Rotational speed required by the motor to drive the gear, rev/min
$RPM_{output}$	Output rotational speed required by the rear wheels to drive the robot, rev/min
$r$	radius of rear wheel, m
$t$	time, s
$t_a$	Time for the robot to reach maximum speed from rest, s

$V_y$	forces acting on point V in the Y direction, where V = A, B, C, and D
$V_{it}$	volume of inner tank, mm <sup>3</sup>
$v_o$	initial speed (rest), m/s
$v_{max}$	maximum speed of the robot, m/s
$W_{it}$	width of inner tank, mm
$W_c$	weight of component, N
$W_{base}$	weight of base, N
$W_{Main\ arm}$	weight of main arm, N
$W_{Connector}$	weight of connector, N
$W_{Horizontal\ arm}$	weight of horizontal arm, N
$W_{support}$	weight of gripper support, N
$W_{Gripper}$	weight of gripper set, N
$X$	horizontal distance of centre of mass from the robot side, mm
$x$	spring stretch or compression, mm
$x_{cg}$	centre of gravity in X direction relative to a point, mm
$x_n$	centre of gravity of that component n in X direction relative to a point, mm
$Y$	vertical distance of centre of mass from the floor, mm
$y_{cg}$	centre of gravity in Y direction relative to a point, mm
$y_n$	centre of gravity of that component n in Y direction relative to a point, mm
$z_{cg}$	centre of gravity in Z direction relative to a point, mm
$z_n$	centre of gravity of that component n in Z direction relative to a point, mm
$\alpha$	angular acceleration, rad/s <sup>2</sup>
$\tau$	Torque, N·m
$\tau_{input}$	Torque required by the motor to drive the gear, N·m
$\tau_{output}$	Output torque required by the rear wheels to drive the robot, N·m
$\tau_{part\ 1\ \&\ 2}$	torque required for part 1 and part 2, N·m
$\tau_{part\ 3}$	torque required for part 3, N·m
$\omega$	angular velocity, rad/s
$\theta_{slope}$	Maximum slope incline to travel, °

$\theta_{topple}$	topple angle,
AI	Artificial Intelligent
DC	Direct-current
DoF	Degree of Freedom
FEA	Finite Element Analysis
IoT	Internet of Things
PLA	Polylactic Acid
RPM	Revolution per minute
3D	Three-dimensional
4WD	Four-wheels-drive

## **CHAPTER 1**

### **INTRODUCTION**

#### **1.1 Background**

Technology has developed and evolved significantly over several decades, revolutionising many different fields and industries and these technologies are employed in our daily lives. One of the technology advancement is robotics. According to Moravec (2022), robots are machines that run autonomously and are able to eliminate the need for human labour to carry out tasks. Even though the appearance of robots does not look like humans, they can carry out activities in a way that is human-like. The term "robot" was first used in the play R.U.R. (Rossum's Universal Robot) by Karel Apek (1920), which was taken from the Czech word "robota" with the definitions of "forced labour" and "serf". According to The Robotic Industries Association (RIA) (2017) and to Inc. (2020), described robots as "reprogrammable, versatile manipulators designed to move material, parts, tools, or specialised devices through variable programmed motions for the performance of a variety of tasks".

The agricultural robot being developed in this project is a latex cup collector robot, which is categorised under "mobile" and "service" robots. According to Ben-Ari (2018), depending on operating environments, robots are often divided into fixed robots and mobile robots. These two distinct robot types demand quite different capabilities due to their highly varied operating conditions. The majority of fixed robots are industrial robotic manipulators that operate in environments that have been specially designed for robots. Robotic manipulators are now employed more

frequently in less regulated environments, such as highly precise surgery, as sensors and technologies for human-robot interaction get more advanced. Mobile robots, on the other hand, can manoeuvre and carry out duties in huge, vague, and unpredicted settings that were not created with consideration of robots. They must cope with circumstances that are uncertain and ever-changing. Robotic vacuum cleaners and self-driving cars are two examples of mobile robots. Additionally, industrial robots and service robots are two other categories of robots. Industrial robots carry out production-related activities in predetermined environments, whereas service robots help people in completing work.

According to Uribe-Holguin (2020), as reported by the International Labour Organization, the number of people employed in agriculture has decreased dramatically from 44 % in 1991 to 21 % today. An increase in larger farms due to market consolidation and investment in machinery and technology has led to such a workforce exodus. The agricultural sector has always required a lot of human effort to finish tasks. With the implementation of automation, the quality of crops produced can be raised by reducing variation and increasing consistency. Besides, automation is also required to maintain operational continuity due scarce labour supply and high labour expenses. Furthermore, according to the Robotic Industries Association (RIA) (2017), the UN predicts that there will be 9.7 billion people on earth in 2050. The demand for food and other natural resources will increase significantly, and farmers will be under tremendous pressure to meet the demand. Farmers' output yields can increase with the development of agricultural robots. For example, rubber is highly demanded as it can be used to produce various types of products such as gloves, tyres, footwear, mattresses, and so on. Therefore, due to the wide range of opportunities rubber can provide, it is crucial to invest in agricultural robots for rubber plantations. The development of automatic latex harvest is crucial for the rubber industry to get over the development snag.

## 1.2 Problem Statements

The rubber sector encompasses natural rubber which is produced from the latex of plants, as well as synthetic rubber, which is a man-made material created from petroleum. 93 % of the natural rubber produced worldwide is produced in Asia, with Thailand topping the list, followed by Indonesia and Vietnam. Other countries such as India, China and Malaysia are also significant rubber-producing countries in Asia (Dublin, 2020). Based on the data provided by the Malaysian Rubber Council (MRC) (2021) from year 2020 to year 2021, global production and consumption of rubber grew by 7.3 % and 10.6 % respectively. Although both production and consumption of rubber resulted in a huge increment, however the total rubber production is 29.4 million tonnes and the total rubber consumption is 29.7 million tonnes. This shows that the demand for rubber is much higher than the amount produced which leads to shortage of raw materials for rubber industries to produce goods. Malaysia, as one of the largest rubber producers around the world, saw a slight reduction of 4% in rubber production and an increment of 4.8 % in rubber consumption from year 2020 to 2021. Malaysian rubber consumption has surpassed Malaysian rubber production over the last five years.

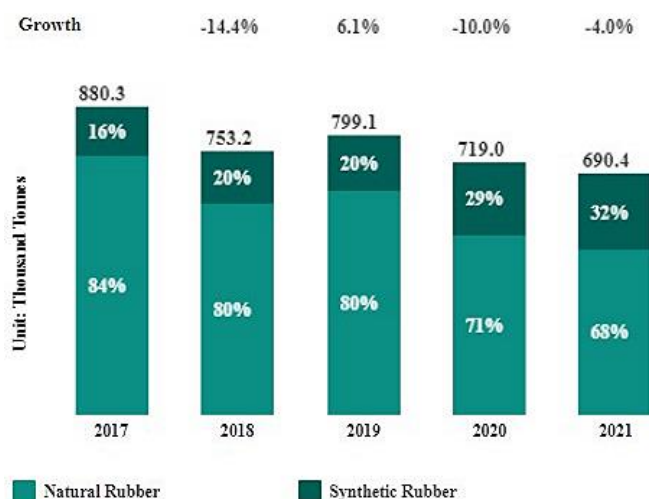


Figure 1.1: Rubber Production in Malaysia from year 2017 to 2021 (in thousand tonnes) (Source: MRC, 2021)

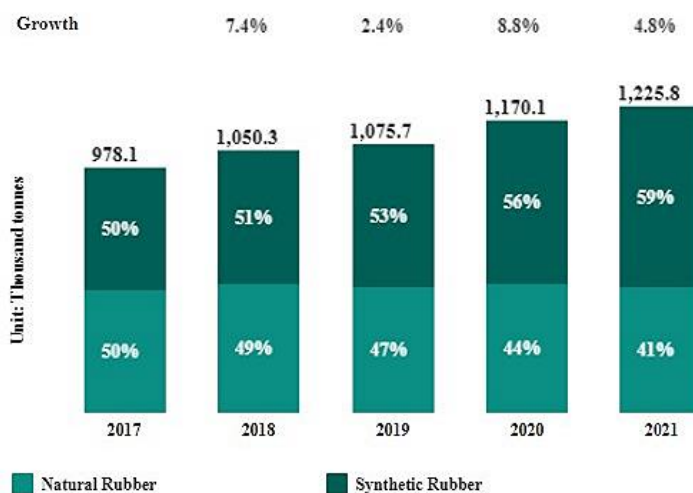


Figure1.2: Rubber Consumption in Malaysia from year 2017 to 2021 (in thousand tonnes) (Source: MRC, 2021)

The issues that led to Malaysia's low rubber production are discussed below. The major factor that leads to low rubber production is the reduction of a significant amount of the work force (Wang, 2022). The root cause of the reduction in the work force on rubber plantations is the health problems of workers. Each worker is required to chop up to 500 trees every tapping morning, which is between 2 a.m. and 6 a.m., when the latex yield is higher. Workers still needed to gather each tree's latex after their breakfast. Their health issues could be put in danger by demanding such a heavy physical workload (Zhou, 2021). Musculoskeletal disorders are one of the most significant health issues present among labourers on rubber plantations. As the land of the rubber plantation is uneven, the workers will require more energy to maintain balance when they tap and collect rubber latex. In addition, most of the rubber tappers are old, and some of them may be overweight (Doi, 2014). The number of young individuals working in agriculture is still quite low. The primary reason behind this phenomenon is that the work in agriculture is tough, challenging, and low-profit (Borneopost, 2019). This has led to a lower performance of the rubber workers and resulted in lower rubber production (Doi, 2014). Furthermore, the coronavirus outbreak resulted in a spike in demand for natural rubber products such as latex gloves and other latex medical products (Ginger, 2021). Rubber plantations are a labour-intensive sector. However, as the containment measure went into force by restricting economic activities and affecting livelihoods due to the COVID-19

pandemic, the number of workers allowed to work was limited, which led to low rubber production.

### **1.3 Aims and Objectives**

Below are the objectives of this project:

- i. To build a mobile robot with a 5 Degree of Freedom (DoF) motion robotic arm that can move across a variety of terrain surfaces and pick up the latex cup from various heights.
- ii. To study and analyse the robot prototype design by utilising Solidworks's Finite Element Analysis (FEA) and Motion Study Analysis.
- iii. To create and build a functional robot prototype using a 3-Dimensional (3D) printer.

### **1.4 Scope of Project**

The project scope is to create and develop a mobile robot which is highly accurate, stable and flexible. A latex cup collector robot was created after careful planning, research, and analysis. The pick, pour, and place repetitive task-perform ability of the robot prototype was examined. Besides, the robot prototype's stability and availability were tested on uneven terrain.

The study's constraints were the prototype's size and material cost, therefore, all the decisions were very prudent. The latex cup collector robot parts were printed using a 3D printer as the components are in small dimensions and cannot be found on the market. The sizes of the prototype components were restricted to 200mm due to the size limitation of the Raise3D N2 printer. In order to stay within the project's budget, the prototype's design specifications were carefully taken into account.

## CHAPTER 2

### LITERATURE REVIEW

#### 2.1 Latex

Latex is a white, milky sap that can be found under the bark of the rubber tree. Latex can be naturally produced by plants and can also be synthesised through chemical operations. Although the rubber tree is the most well-known source of natural latex, in fact, all the trees around the world consist of around 10 % latex. Natural latex is a combination of proteins, starches, sugars, resins, oils, tannins, alkaloids, and gums. Latex is a protection mechanism for the plant to defend itself against insect attacks. When latex comes into contact with air, it will coagulate. The latex harvesting process can be started once a rubber tree reaches maturity, which is around the age of 7 when it is able to produce rubber. The first step in harvesting latex is the tapping process. The tapping process is to make a small cut in the bark of the rubber tree to allow splitting of the bark. The splitting of the bark of the tree will allow the latex to flow out and be collected. The latex will flow into the cup that is fastened to the end of the tree cut. After that, latex from the trees is poured and collected in a tank. To keep latex from coagulating after collection, some chemicals are added to the latex (Liné, 2020).



Figure 2.1: Rubber tree latex (Source: Liné, 2020)

## 2.2 Automated Agricultural Harvesting

Agricultural robots are able to conduct repetitive, sluggish, and boring work for farmers so that they can concentrate on how to increase total output yields. Harvesting and picking, weed control, phenotyping, sorting, and packing, utility platforms and autonomous mowing, pruning, seeding, spraying, and thinning are some of the most frequent tasks performed by robots in agriculture. Harvesting and picking are two of the most often employed robotic applications in agriculture because of the speed and precision that robots can achieve. This contributes to boosting overall output yield and reducing crop waste (ROBOTIC INDUSTRIES ASSOCIATION (RIA), 2017). According to Gossett (n.d.), several studies have been done on agricultural robots. Examples of agricultural robots are lettuce harvesting robots by the University of Cambridge, strawberry harvesting robots by the Co-founder of Harvest CROO, and weeding machines. In the development of a strawberry harvesting robot, rather than using a single arm, it utilizes an assortment of robotic components to select the berries and pack them. The strawberries harvesting robot also employs computer vision to distinguish between ripe and unripe berries. In addition, the robot can reportedly pick a crop in eight seconds and proceed to the next in one-and-a-half, which is speedier than human employees.

### 2.3 Obstacles in Deploying Agricultural Robot

Increasingly more people are beginning to realise the possibilities of agricultural automation with the quick advancement of technology, together with the growing technological robustness and trust-building capability of robots. However, the agricultural sector has been slower to become automated compared to other sectors. One of the factors causing the low adoption of agricultural robots is the insufficient trust of farmers. In contrast to other industries, the agricultural sector has lower returns and may only have one chance to plant and harvest per year. If the agricultural robots fail to operate, the farmers may lose their annual income. Therefore, farmers are cautious about deploying these agricultural robots unless they have enough technical robustness and reliability to eliminate the potential threats. Another reason for agricultural robots' low adoption is their high initial cost. The initial investment cost for robots is still a huge financial pressure for farmers, even though the cost of purchasing agricultural robots has been reduced over the past few years. Another cost that may be a burden for the farmers is the maintenance cost of the robots. In addition, lack of geographical accessibility is also one of the factors contributing to the low adoption of agricultural robots. Geographical accessibility issues have been brought on by a lack of IT infrastructure. Although agricultural robot technology has advanced over the past few years, widespread adoption is still a long way off. Communication systems such as Wi-Fi, cellular, and so on are one of the main problems of agricultural robots. Farms are often found in rural areas with very little infrastructure, which makes it difficult to support communication networks (Claver, 2022).

The application of agricultural robots is still a challenging task. For example, a robotic harvesting system for sweet peppers has many obstacles. When confronted with challenging circumstances such as the existence of dust, varying intensities of light, thermal gradients, and motion brought on by the breeze, vision systems need to be capable of finding and accessing the pepper's level of maturity. However, sophisticated visual technologies alone are still insufficient for pepper harvesting. To precisely grasp and position a pepper, a robotic arm needs to manoeuvre across hazardous terrain. When compared to sorting and positioning metal pieces on an assembly line, this approach is much more challenging. The agricultural robotic arm

needs to be precise to harvest the peppers without damaging them while at the same time being flexible to adapt to changing circumstances (ROBOTIC INDUSTRIES ASSOCIATION (RIA), 2017).

## 2.4 Components of Agricultural Robot

In general, agricultural robots are developed to carry out their "main task," which is typically a particular agricultural task like seeding, weeding, picking, harvesting, etc. Agricultural robots are made up of several systems and technologies to function and complete tasks. Agricultural robots need to be capable of carrying out a variety of "supporting tasks" such as localization and navigation, object identification, etc., to complete the "main task". Transfer of data and commands takes place between the agricultural robot systems, regulating the "supporting tasks" and "main tasks" to ensure the system operates effectively. The main components for agricultural robots to be able to function are mobility and steering, sensing, path planning, and manipulation (Bechar, 2016).

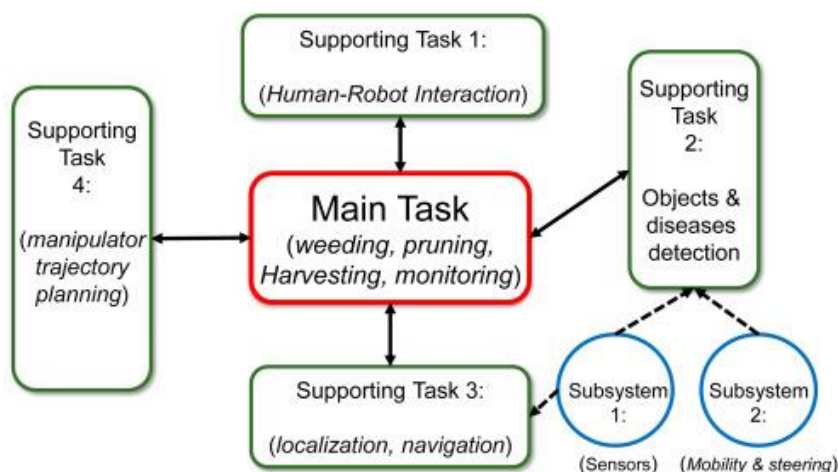


Figure 2.2: Structure of task sub-systems in an agricultural robot (Source: Bechar, 2016)

## **2.4.1 Mobility and Steering**

When a mobile agricultural robot system is involved in motion planning, its basic functionality is seen as a dynamic process that involves contact between the robot and its immediate surroundings. By interacting with the soil, the steering and mobility subsystems of the agricultural robots have to work together to manoeuvre the robot at the right speed and in the right orientation. The development of agricultural robots must take into account a number of factors, which include the ability of the robot to function throughout damp environments without becoming stuck or harming the soil structure and also having a flexible robot frame or platform, which lowers complexity while allowing all wheels to interact with the ground (Bechar, 2016). There are a few alternatives for the mobility of agricultural robots, which include legs, wheels, wings, rail tracks, or drones. Locomotion, steering, and suspension are the three sub-functions that make up a robot's mobility. These sub-functions carry out various tasks to construct a whole mobility subsystem.

### **2.4.1.1 Transmission**

The types of transmission that have been proposed for robots are chain drive, direct drive and differential drive.

Differential drive systems have individual actuators for each of their two wheels. Typically, the driving wheels are positioned towards the front of the robot on each side. The benefits of a differential drive system include simplicity and direct connection of the driving wheel to the motor, which is typically a gear motor, as most gear motors lack the torque necessary to drive a wheel directly. However, one of the drawbacks of a differential drive system is that moving the robot in a straight line is challenging as the wheels are independent. As the driving wheels are independent, the robot will lean in one direction if they are not rotating at precisely the same rate. Owing to minor variations in the driving motors, friction variations in the drive trains, and friction variations at the wheel-ground interaction, it is difficult to get the driving motors to rotate at an equivalent pace. To make sure that the robot

is moving straight, odometry sensors can be used to obtain exact wheel position information and modify the motor RPM (Costanzo, 2021).

Chain drives can be used to mechanically transmit power from one location to another. It is commonly used in vehicles like bicycles and motorcycles to transmit power to the wheels. The most common method of transmitting power is by a roller chain, often referred to as a drive chain or transmission chain, which travels over a sprocket gear and interacts with holes in the chain's links as it moves over the gear (Khurmi, 2005). One of the advantages of chain drive is the ability to prevent slippage since the teeth on the sprocket properly align with the holes in the chain links. Due to the absence of slipping, chain drives can transmit power with an efficiency as high as 98%. However, there are numerous disadvantages of chain drive which including the expensive cost, the need for cautious maintenance and potential for velocity variations brought on by excessive stretching (Anjum, 2012).

Direct drive can directly transmit power to the locomotion system and then to the wheels without the need for transmission components like gears, chains or pulleys. The advantages of direct drive are low maintenance requirements as there is no wear on tools, superior dynamic performance and precise positional control. Direct drive is suitable for straight moving, however, if turning is necessary, the robot's inner wheels may experience slippage issues or the robot may turn in an unsteady state due to the varying path lengths of the inner and outer wheels (Hoogewijs, 2020).

#### **2.4.1.2 Locomotion**

There are three types of locomotion that are commonly used in agricultural robots to adapt to the agricultural environment: leg locomotion, wheel locomotion, and track locomotion.

Robots with legs for locomotion are suitable in agricultural fields due to their flexible movements towards the terrain present in the agricultural fields. They are

incredibly adaptable and can move through a variety of terrain, including rocky and uneven terrain (Fue, 2020). In the research study by Zhang (2019) about the implication of head movement adjustment on the goats' stability, as the slope increases, the trajectory of the head of the goat (representing the robot platform) will abruptly fluctuate to achieve balance and stability when walking. When the goat moves on different slopes, the head of the goat will fluctuate in vertical motion to achieve stability. The fluctuation increases as the slope increases. This proves that leg locomotion is not suitable for robots that require liquid transport. Besides, some of the drawbacks of leg locomotion are poor energy efficiency, a relatively slow pace, and high complexity and costs due to large numbers of actuators, sensors, communications, and auxiliary hardware. Furthermore, they are often sluggish and much less energy efficient compared to wheeled and tracked locomotion robots (Tedeschi, 2014).



Figure 2.3: Example of leg locomotion system (Source: Tedeschi, 2014)

Wheel locomotion has a high speed, making field navigation faster and more practical (Fue, 2020). According to research, most agricultural robots use wheels as their locomotion system, especially four-wheel-drive (4WD). However, local geographical conditions like rocks and braches have a significant impact on wheeled systems. Additionally, the frequent movement of these agricultural robots across the farm could lead to a significant level of soil compaction (Oliveira, 2021). Research

has been done to resolve the issues of wheel locomotion for travel on unstructured terrain. For instance, Nakajima (2011) has proposed a wheeled robot with separated front and rear wheels. The front and rear wheels are separated by two independent moving axles that can turn in any vertical direction when confronted with obstacles or moving on uneven surfaces.

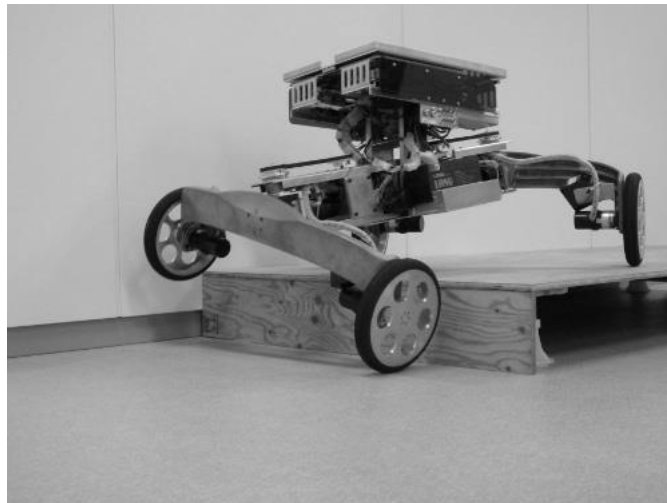


Figure 2.4: RT Mover (source: Nakajima, 2011)

Last but not least is track locomotion. It is suitable for operating in soft and slippery terrain such as sand and mud to prevent sliding as it has a large ground contact area (Bruzzone, 2022). However, there are some downsides to track locomotion, which has a slow moving speed and requires a large amount of energy. Since the lateral track profile of tracked robots is a polygon with moving vertices, they are susceptible to vibrations and are rarely equipped with dampening mechanisms, which will restrict the maximum speed and lower mechanical performance (Bruzzone, 2012).

### 2.4.1.3 Steering

There are three types of steering that can be applied to robots, including Ackermann steering, four-wheel steering, and skid steering.

Ackermann steering is also known as kingpin steering (Hrbacek, 2010). The Ackermann steering principle serves as the foundation for the steering control system of a four-wheeled vehicle (Xu, 2021). Robots are able to operate efficiently and behave well at high speeds by using differential drive systems in conjunction with Ackermann steering (Hrbacek, 2010). In the Ackermann mechanism, the front wheels of the vehicle are connected with a tie-rod to allow the wheels to turn at different angles so that the wheels are independent when turning (Skill-Lync, 2022). The angle of each wheel will be different during the turning of the vehicle as each wheel will travel over a different radius, requiring the inner wheel to be slanted more than the outer wheel (Hrbacek, 2010). Therefore, the Ackermann steering system can be applied to the coordinated motion control of agricultural robots to greatly reduce tyre sideslip during turning and travel at high speeds. When the wheels turn, the angle of the end of the pivot in the double pivot system can intersect at the centre of rotation due to its alignment with the axis of Ackermann and the centre of the rear axle (Hrbacek, 2010).

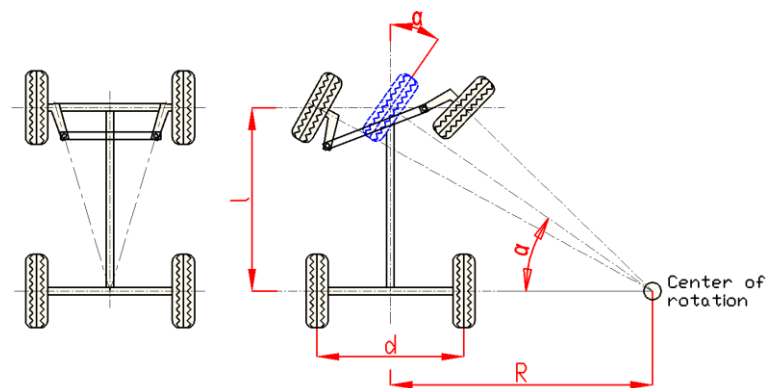


Figure 2.5: Ackermann steering principle (Hrbacek., n.d.)

Four-wheel steering can also be known as rear-wheel steering or all-wheel steering. Four-wheel steering will actively direct the rear wheels during the turning of vehicles. Four-wheel steering can create near-neutral steering and can automatically correct an understeer or oversteer issue. In addition, a four-wheel steering system can allow a tighter turn, enhance the steering response and stability of the vehicle, and have higher efficiency compared to Ackermann steering (Sundar, 2018). However, a large number of motors are required for four-wheel steering to operate compared to Ackermann steering. This will increase the weight of robots and

power consumption and, at the same time, increase the complexity of control system algorithms.

Next, the skid steering mechanism is based on the movement of each wheel of the vehicle in different directions and velocities, which causes the wheels or tracks to skid or slip. Due to their adaptability and simple design, skid-steered robots will be significant in agricultural robotics. However, the inherent non-linearities of skid steering have caused the design of the controller to be extremely challenging. Besides, because of the abnormalities in the agricultural land, the system's dynamics are continually changing (Fernandez, 2018). Another drawback of skid steering is that it can be challenging to maintain the required speed for all four wheels in order to travel straight (Costanzo, 2021).

#### **2.4.1.4 Suspension**

A suspension is a network of links that joins the car's chassis to its wheels. The main function of suspension is to maintain constant contact between the wheels and the ground, which promotes the stability and traction of the vehicle. The types of suspension that will be discussed are spring, double wishbone, and Rocker Bogie.

Double wishbone suspension is a suspension system with two control arms (also known as wishbones) that are connected to the wheel knuckle and spindle. Each wheel is able to move up and down on the driving wheels because the axle-shafts are connected to the differential and hub flanges. In front-wheel-drive applications, it additionally enables steering movement in side-to-side directions. Double wishbone suspension is usually installed with a shock absorber between the upper and lower control arms to minimize the suspension bounce (OnAllCylinders, 2017). Double wishbone suspension provides good stability and consistency for vehicles. According to research done by Faurox and Bouzgarrou (2011) related to the vehicle with double wishbone suspension travelling over obstacles, they found out the stability limit of the double wishbone. They carried out experiments by allowing the robot to travel at various speeds and heights. The robot with double wishbone suspension is only able

to travel over low obstacles at high speeds and over high obstacles at low speeds. This illustrates the non-linear relationship between robot speed and obstacle height. If the robot travels over low obstacles at low speed and high obstacles at high speed, it will tip over. To resolve this problem, they suggested using sensors to determine the height of the obstacles to control the speed of the robot.

The spring is significant in adjusting the inconsistencies of vehicles, keeping the suspension system at a prescribed height and being able to sustain extra weight without excessive drooping (Goms, 2011). The coil spring allows the vehicle to remain stable as it stretches when the wheel moves down and compresses when the wheel moves up. Dampers, often known as shock absorbers, contain a piston that goes vertically with the wheel's movement. By adopting a damper in the suspension system, the wheels of the robot can still remain on the ground even if the robot is slanted, which shows that it provides good stability to the robot. However, the robot is not able to return to its initial position. But the problem of not being able to return to the original posture can be solved by adding springs to the suspension system with a damper (Roh, 2013).

The Rocker Bogie is a suspension system developed by NASA, and this suspension system was implemented in their Mars rover. "Rocker" refers to how the large links on either side of the suspension system rock when they are in motion, while "Bogie" refers to the links with a drive wheel at either end. Rocker Bogie is a suspension system that has stub axles and is springless, which enables the rover to pass across obstacles that are almost double the size of the wheel diameter while at the same time maintaining contact with the ground with all six wheels. However, the height of the centre of gravity has limited the tilt stability of the rover. Besides, the Rocker Bogie suspension system was made to operate at slow speeds of about 10 cm/s in order to reduce dynamic shocks and subsequent damage to the vehicle when navigating over large obstacles (Technology Robotix Society, 2019).

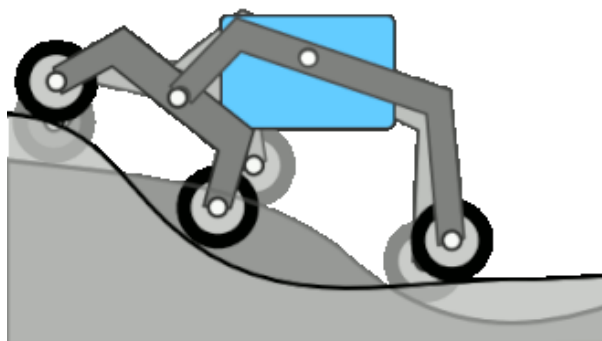


Figure 2.6: Rocker-bogie suspension system (Source: Technology Robotix Society, 2019)

### 2.4.2 Manipulation

A manipulator is typically an arm-style piece of electromechanical machinery that can operate in a confined area, and the end of the manipulator is equipped with an end-effector. Manipulators are categorised based on different degrees of freedom, joint type, length of the link and length of offset. A manipulator's main job is to position its end effector such that the end effector is able to grasp the work object and to posture it so that it can accomplish the task required. Robotic arm manipulators are commonly found in industrial robots. However, they are unsuitable for agricultural use due to their enormous weight, high costs, and high power consumption. Thus, a manipulator for agricultural use ought to be made in a straightforward, fundamental manner. The mechanism of the end effector is chosen according to the task to be carried out, the environment, and the object to be manipulated. Sensors are required to be equipped on the end effector when it requires physical contact with the crops to avoid injuring them. This is due to the fact that crops are normally much softer than normal objects in industrial sectors and crops come in various sizes and shapes (Bechar, 2016). The manipulator and end-effector are the two sub-functions that make up a robot's manipulation system. A manipulator serves as an indicator for the end-effector as it approaches the work item and

completes its duty. Thus, in order to function precisely, the design concepts for the manipulator and end-effector should be connected.

#### **2.4.2.1 Manipulator**

There are three manipulators that will be discussed in this section, which are pneumatic manipulators, hydraulic manipulators, and motor-driven manipulators.

Pneumatic manipulators are manipulators that use pneumatic actuators to operate. Pneumatic actuators produce force when the cylinder moves along the axis of the piston due to a rise in pressure. When a spring-back force is supplied to the piston or fluid is supplied to the opposite side of the piston, the piston will then return to its initial position. Although pneumatic manipulators ensure high accuracy and repeatability, their efficiency is lower due to loss of pressure and air compressibility.

Hydraulic manipulators have the same operating principle as pneumatic manipulators; the difference between them is that the hydraulic manipulators use an incompressible liquid instead of compressed air. Due to fluid incompressibility, hydraulic manipulators can maintain force and torque without the pump contributing additional fluid or pressure. However, the downside of hydraulic manipulators is that they will have leaking problems, which may lead to damage to components.

Last but not least is the motor-driven manipulator; it can provide higher precision and operate faster compared to pneumatic and hydraulic. In addition, motor-driven manipulators are able to control position, velocity, applied force, and torque. The disadvantage of motor-driven manipulators is that tool wear may occur due to overheating of the continuously running motor (Gonzalez, 2015).

### **2.4.2.2 End-Effector**

The two types of end-effectors that will be discussed are electric grippers and vacuum grippers.

Robotic applications such as pick-and-place and machine tending commonly employ electric grippers. Electric grippers are ideal due to their moderate gripping force and high speed. Electric grippers commonly have two or three jaws, which makes three jaw grippers the best choice when handling cylindrical or round items.

Vacuum grippers lift, handle, and manipulate things using the difference in pressure between air pressure and vacuum. Vacuum grippers offer the benefit of being able to handle a range of objects when compared to other grippers. However, vacuum grippers require additional electricity to operate due to the usage of compressed air and they are sensitive to dusty environments, which may lead to a reduction in performance (Universal Robots, 2022).

### **2.4.3 Sensing**

Sensors are utilised in various types of tasks, which include mapping, localization, navigation, plant detection, and environmental parameter monitoring. They help with decision making, operations, and the performance evaluation of the robots. There are two types of sensors: internal sensors and external sensors. The robot's inertia, speed, and accelerations are measured via internal sensors. For instance, gyroscopes are used to determine the rotational acceleration. In contrast, external sensors gather ambient data regarding the state of the system relative to the location of the robot. Machine vision, GPS sensors, laser radar (LIDAR), and ultrasonic waves are a few examples of external sensors (Bechar, 2016).

#### **2.4.4 Path Planning**

Path planning is seen as one of the components of navigation, and constitutes one of the most prevalent and essential "supporting tasks" for agricultural robots. It is important in the advancement of agricultural robot systems since it determines the best route for the robot to go from one location to another while also avoiding impediments in its way (Bechar, 2016). Path planning depends on the crops and requires the collaborative effort of sub-systems such as manipulators, sensors, and end effectors to perform effectively. Path planning gets expensive to protect the plants from damage if the branches are weak or the fruits are extremely delicate and the degree of freedom of the robotic arm is high. The majority of the agricultural robots reported using GPS and cameras along with path tracking algorithms to operate around the farm (Fue, 2020).

#### **2.5 Improvement from Previous Research**

According to research done by Kang (2021), a latex cup collector robot prototype with 3 DoF was being designed and developed. The prototype was able to perform the actions of collecting, pouring, and placing the latex cup back in its initial position. However, the availability of the prototype on unstructured terrain was not tested in this research. Other than unstructured terrain in rubber plantations, the latex cups may be located at different heights, which cause the 3 DoF robotic arms to not be able to collect latex cups at different heights. Another research was done by Khor (2022); a latex cup collector robot prototype with 4 DoF was being developed. The robot prototype developed is able to collect latex cups at different heights. In this project, a robot prototype with 5 DoF of robotic arm will be designed and developed by improving on the previous design. The aim of improving on the previous design is to reduce the cycle time for the latex cup collecting process. Besides, to improve the accuracy of the movement of the prototype, an encoder sensor was installed to detect the angle of rotation of the robotic arm.

## CHAPTER 3

### METHODOLOGY

#### 3.1 Chosen Design

Table 3.1 below shows the chosen sub-functions to be used to design the latex cup collector prototype. Then, the prototype will be designed using software called Solidworks.

Table 3.1: Selected mechanisms for each design sub-function

<b>Sub-function</b>	<b>Mechanism</b>
Transmission	Differential
Locomotion	Wheel
Steering	Ackermann
Suspension	Double wishbone and spring
Manipulator	Motor Driven
End-effector	Gripper

#### 3.2 Design of Robot Prototype and Choice of Material

The robot prototype was created in a 1:10 ratio to the original product. The prototype's parts were created in scale with commercially available products. The

selected mechanism for each sub-function will be displayed and thoroughly explained in subchapter 3.2.

### 3.2.1 Properties of PLA Plastic Material in Solidworks

A 3D printer will be used to create the final robot prototype design. The material used in the 3D printer to build the prototype is polylactic acid (PLA) plastic. The properties of PLA plastic were manually entered into the software for simulation and analysis as the Solidworks software did not support the PLA plastic material. Figure 3.1 below displays the properties determined by Matweb (2020), including density, tensile strength, and elastic modulus.

Model Type: Linear Elastic Isotropic  Save model type in library

Units: SI - N/mm<sup>2</sup> (MPa)

Category: plastics

Name: PLA

Description:  

Source:  

Sustainability: Undefined Select...

Property	Value	Units
Elastic Modulus	3800	N/mm <sup>2</sup>
Poisson's Ratio	0.36	N/A
Shear Modulus	1287	N/mm <sup>2</sup>
Mass Density	1240	kg/m <sup>3</sup>
Tensile Strength	60	N/mm <sup>2</sup>
Compressive Strength		N/mm <sup>2</sup>
Yield Strength	70	N/mm <sup>2</sup>
Thermal Expansion Coefficient		/K
Thermal Conductivity		W/(m·K)
Specific Heat	1386	J/(kg·K)
Material Damping Ratio		N/A

Figure 3.1: Properties of PLA plastic material in Solidworks

### 3.2.2 Transmission System Design (Differential)

The transmission system used in the robot prototype is differential drive transmission. Differential drive transmission was chosen as it only requires one motor to drive two wheels. Besides, the differential effect of the differential transmission boosts the performance of the robot prototype when encountering unstructured terrain.

Differential gear box was used to transmit the power from the motor to the wheels. It consists of four types of gear that allow the rear wheels to rotate at different paces. Figure 3.2 shows the differential gear in the differential gear box built using Solidworks. The dimension of the differential gear is not designed to the actual dimension as there are limitations to designing small gears in Solidworks. The design of the differential gear was assumed to have no effect on the simulation of the robot prototype in Solidworks. The differential gear was covered by a case and connected to the rear wheels through axles. Figure 3.2.3 shows the differential gear transmission system used in the prototype.

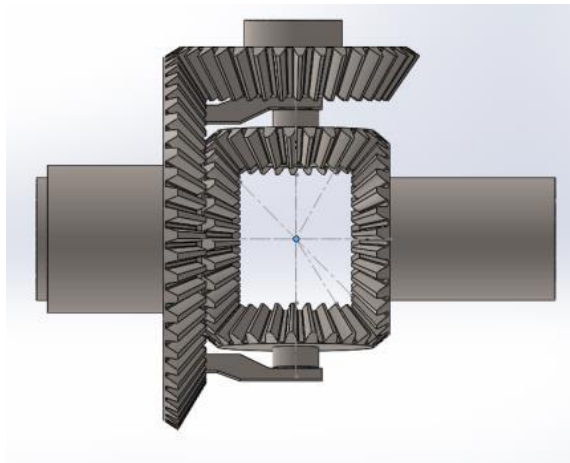


Figure 3.2: Differential gear model in Solidworks

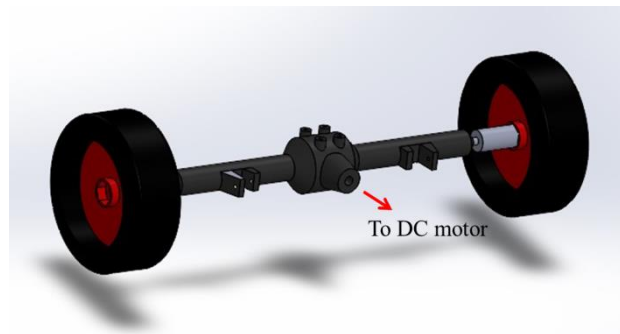


Figure 3.3: Differential gear box in Solidworks

The DC motor was connected to the rear axle of the differential gear box via a propeller shaft, as the DC motor and rear axle are not at the same level. Figure 3.4 shows the connection of the DC motor to the differential gear box for power transmission.

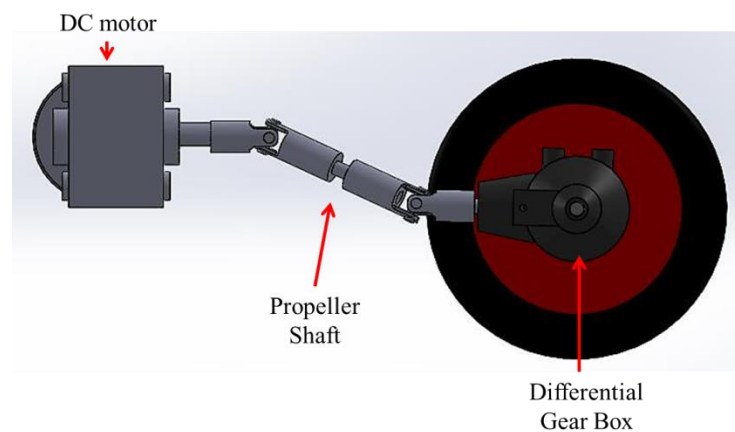


Figure 3.4: Differential gear transmission in Solidworks

### 3.2.3 Locomotion System Design (Wheels)

The locomotion system chosen for the prototype is wheels as they can allow travel at high speed. The dimensions of the front wheels and rear wheels are different. The vehicles in agricultural sector are commonly equipped with larger rear wheels compared to front wheels, as large rear wheels are able to provide better grip on the ground. As the majority of forces are directed at the rear wheel, applying larger rear wheels allows for an even distribution of weight acting on the robot prototype. On

the other hand, according to Sacrewell Farm (2017), the front wheels are usually smaller as they can allow tighter steering angle when turning. Referring to Figure 3.5 and Figure 3.6, the dimension of the front wheel has an external diameter of 65 mm and a width of 24 mm, whereas the dimension of the rear wheel has an external diameter of 85 mm and a width of 31 mm, respectively.

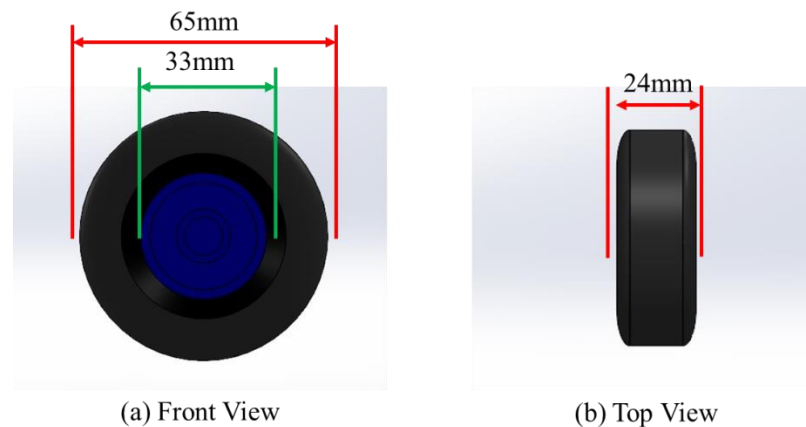


Figure 3.5: Front wheel design

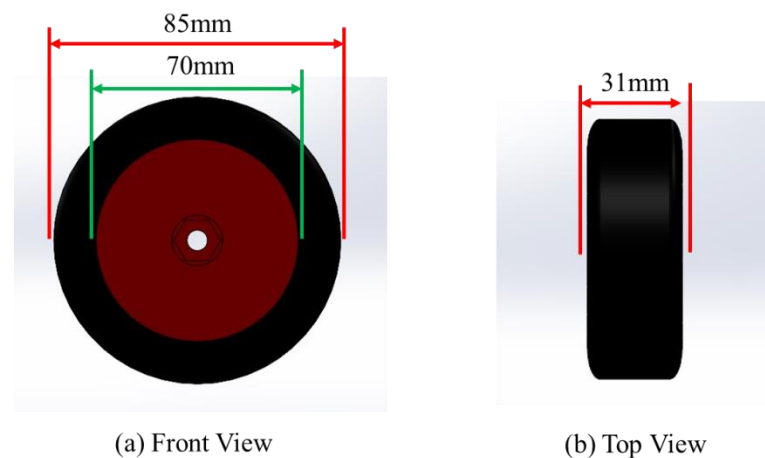


Figure 3.6: Rear wheel design

### 3.2.4 Suspension System Design (Double wishbone and spring)

The suspension system of the prototype featured both double wishbone and spring suspension due to their ability to withstand the external forces occurring on the

wheels. The front wheel system was installed with a double wishbone suspension, whereas the rear wheel system was installed with a spring suspension. Due to the straight orientation of the wheel axle, double wishbone suspension could not be employed on the rear wheel; consequently, spring suspension was used.

The suspension system applied to the front wheel is a double wishbone suspension system. The lower and upper wishbones, two shock absorbers, and wheel hubs make up the double wishbone suspension system. The function of the shock absorbers is to absorb the external forces acting on the wheels, such as when travelling over uneven surfaces. The shock damper can be compressed to a length of 75 mm from its hole-to-hole measurement of 100 mm (refer to Figure 3.7). Figure 3.8 shows the effect of the shock damper acting on the double wishbone suspension system.

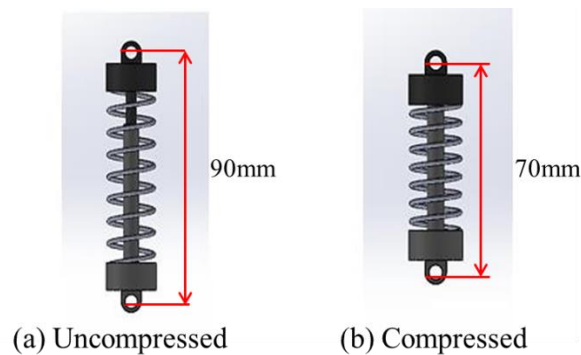


Figure 3.7: Uncompressed and compressed conditions of shock absorber

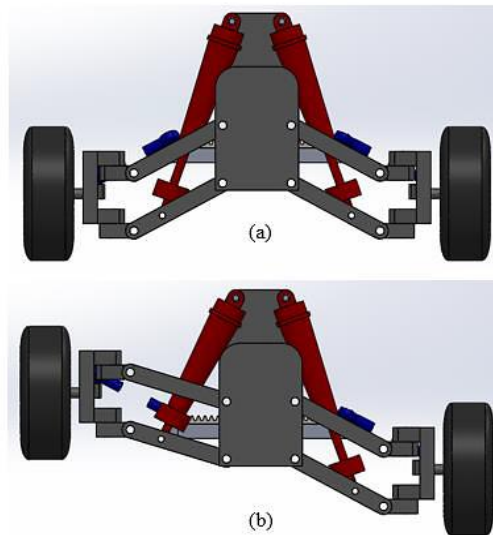


Figure 3.8: Front wheel system: Double wishbone suspension system (a) When both sides are at their initial position; (b) While one of the shock absorbers is compressed

In the rear wheel suspension system, there are two pairs of shock dampers installed to connect the rear wheels to the robot platform (refer to Figure 3.9). The shock absorbers are connected to supporting beams to support the robot platform.

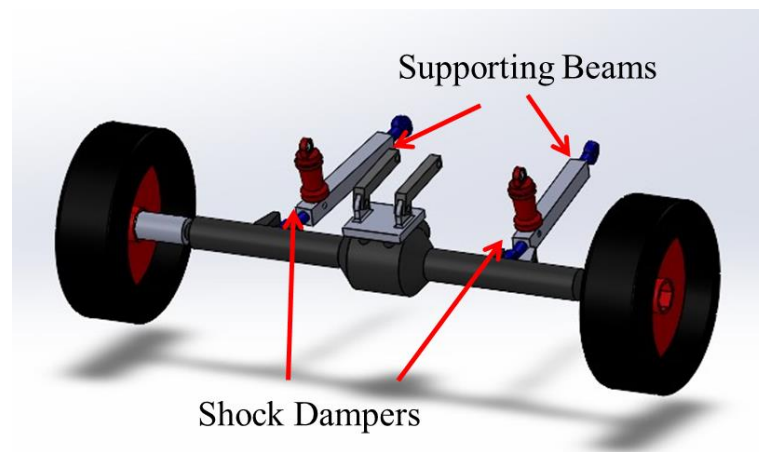


Figure 3.9: Spring suspension system used in the rear wheel

### 3.2.5 Steering System Design (Ackermann Mechanism)

The Ackermann steering system was applied to the prototype as it only requires one motor to control the front wheels. Besides, it also allows sharper turns on the prototype. A steering bar is connected to the steering motor to enable the turning of the front wheels. The wheel hub was designed with an extended arm that connected to the steering bar, allowing the wheels to turn left and right synchronously to accomplish turning (refer to Figure 3.10).

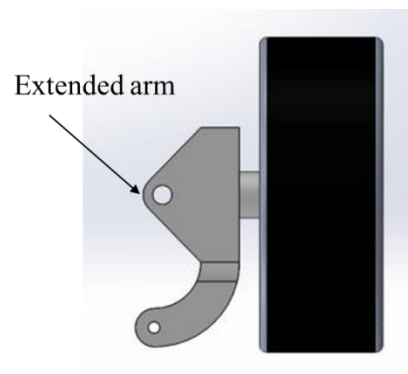


Figure 3.10: Extended arm on wheel hub

To allow the wheels to move freely as they will when they absorb external impact, a linkage was created between the wheel hubs and the steering bar. The linkage was designed with a ball joint and rod. A ball and a socket make up the ball joint (refer to Figure 3.11). While one of the ends is fixed, the ball joint allows rotating movement at either end. Then, a rod was connected with a ball joint at both ends to become a ball joint linkage rod. Figure 3.12 depicts the connection between the steering bar and wheel hubs using ball joint linkage rods.

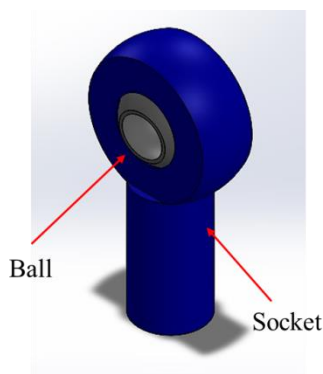


Figure 3.11: Design of ball joint

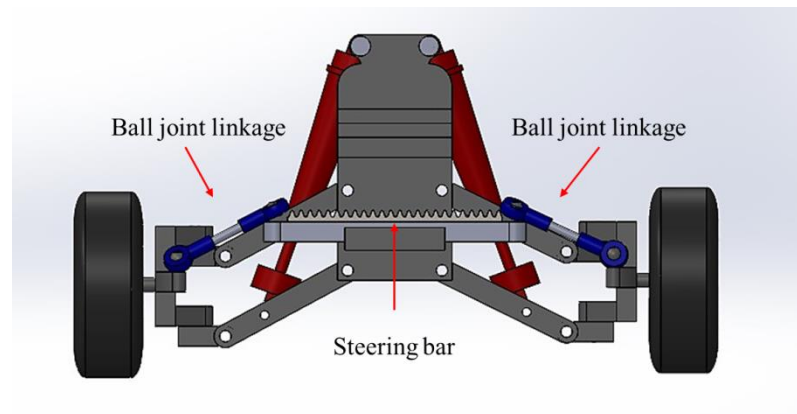


Figure 3.12: Connection between steering bar and wheel hubs using ball joint linkage rods

A DC motor was used to control the steering bar of front wheels. A gear was attached to the DC motor, and its job was to grab hold of the steering bar's rack teeth and convert rotational action to linear motion. Figure 3.13, 3.14 and 3.15 depict how the steering wheel and bar are turned by the DC motor.

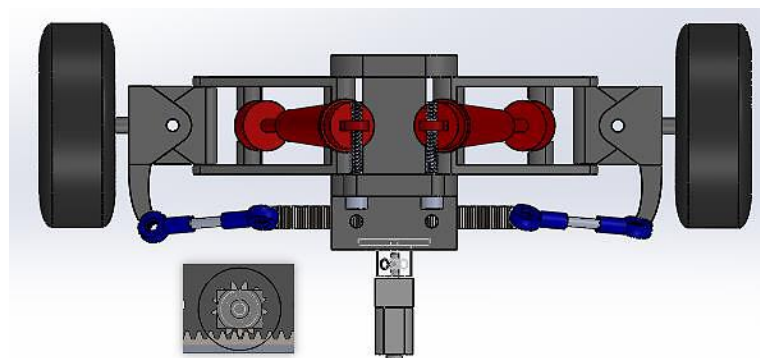


Figure 3.13: Wheels are aligned straight and the gear was set at default position

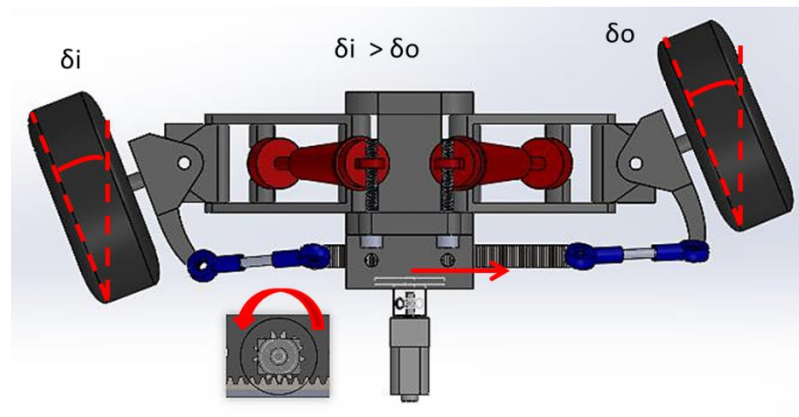


Figure 3.14: Both wheels turn left when the servo motor rotates its shaft anti-clockwise

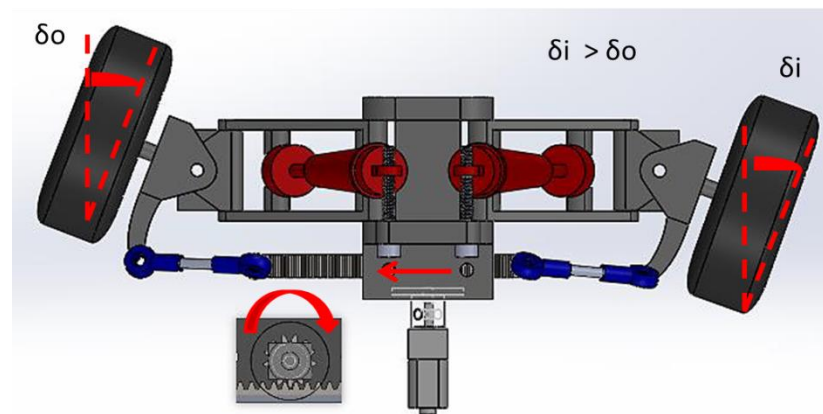


Figure 3.15: Both wheels turn right when the servo motor rotates its shaft clockwise

The principle of Ackermann steering system states that the steering angles,  $\delta$  for both wheels will be different when turning. The inner wheel's steering angle,  $\delta_i$  will be always greater than the outer wheel's steering angle,  $\delta_o$ .

### 3.2.6 Manipulator Design

The robot's primary duty is to collect the latex cups that are positioned at various heights. Therefore, the manipulator ought to be built with a greater joint or with a greater DoF so that it is able to move in both vertical and horizontal directions. The manipulator design for the prototype is 4 DoF. The 5 DoF refers to the manipulator system of the prototype. There will be one more DoF for the end-effector to perform

pouring tasks. Therefore, there is a total of 5 DoF in the manipulator of the robot prototype.

The robotic arm has 3 DoF to move upwards and downwards, which means that it requires 3 motors at each joint to operate. However, this will increase the weight that the robotic arm has to withstand. In order to control the 3 DoF using only two motors, the manipulator design for the prototype was based on the design of "EEZYbotARM MK2" (Carlo, 2018). Figure 3.16 shows the "EEZYbotARM MK2". The horizontal arm and supporting arm are connected to the gripper support by a parallelogram mechanism that was incorporated into the arm design. The horizontal arm and supporting arm are connected to the gripper support by a parallelogram mechanism that was incorporated into the arm design. With this mechanism, the supporting bar will rotate parallel to and in tandem with the horizontal arm. When the manipulator is moving, the mechanism guarantees that the gripper support maintains alignment with the plane. This could also prevent the liquid latex from leaking when collecting the latex cups, as the gripper will stay horizontally. The manipulator design of the robot prototype was also inspired by the "SolidWorks Tutorial" from Youtube (2017).

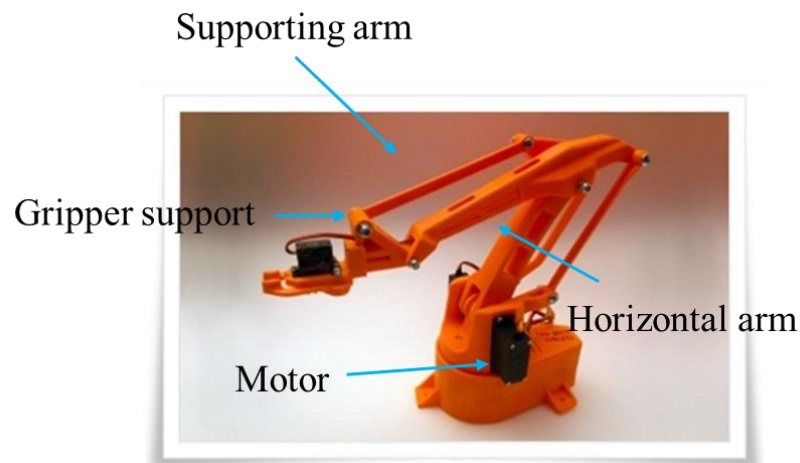


Figure 3.16: EEZYbotARM MK2 (Source: Carlo, 2018)

For the base design, a base with two supporting legs was created to hold the servo motor that allows that robotic arm to rotate in a horizontal direction. Then the shaft of the servo motor will be connected to a rotating base that can rotate in a

horizontal direction. Next, the base for the robotic arm to move in a vertical direction was designed with a blank space in the middle. The blank space was designed to hold the motor so that the centre of mass of the manipulator could be reduced. The main arm is propelled by the right-side motor, while the horizontal arm is propelled by the left-side motor. Figure 3.17 shows the base design of the robotic arm.

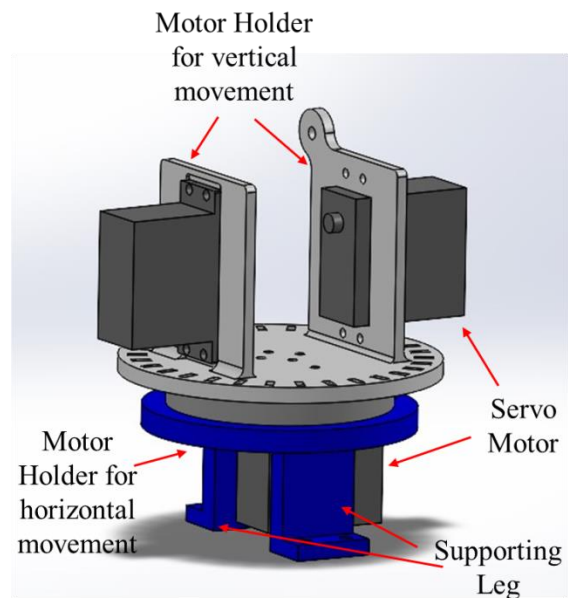


Figure 3.17: Front view of manipulator base design for horizontal movement

The main arm's hole-to-hole distance is 145 mm (refer to Figure 3.18). In order to reach the targeted latex cup, the main arm must be long enough to stretch the horizontal arm and gripper forward. The main arm's perforations at the bottom were made to enable rotation by connecting the main arm to the motor.

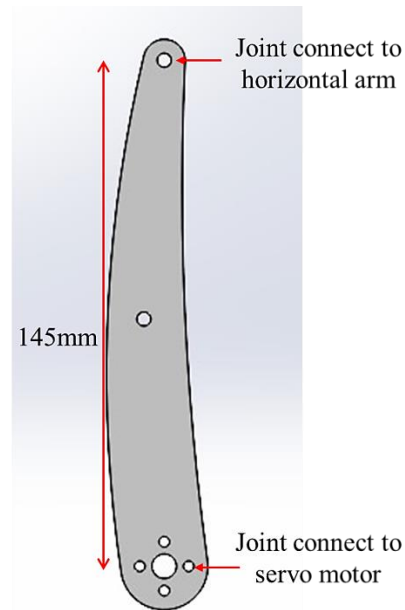


Figure 3.18: Main arm of manipulator system design

The hole-to-hole distance of the horizontal arm is 145 mm (refer to Figure 3.19). From top to bottom, the first joint of the horizontal arm is connected to a linkage bar that will control the movement of the horizontal arm, the main arm is connected to the second joint and the last joint is connected to gripper support.

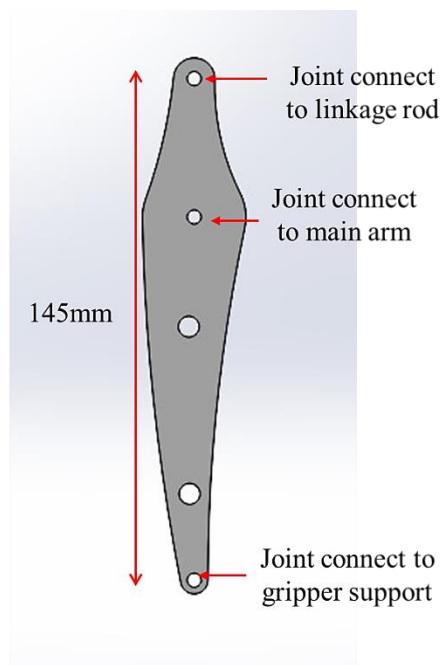


Figure 3.19: Manipulator horizontal arm design

A gripper support was designed to hold the gripper. Besides, it is also used to hold the motor and camera chip (refer Figure 3.20). The cylindrical bar at the bottom of the gripper support is to hold the gear and gripper; the gripper will rotate with the gear to pour liquid latex into the tank.

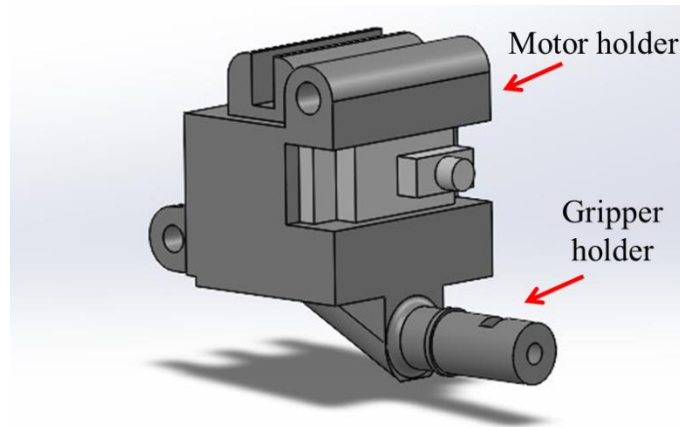


Figure 3.20: Gripper support design

In addition to these parts, there are numerous other parts that are made to work in support of the primary parts. Most of these components are linkage rods that hold the primary components in place.

### 3.2.7 End effector Design (Gripper)

The prototype design's end-effector was a gripper end-effector. The gripper end-effector uses less power, has a faster processing time, and is not affected by dust. The dimensions of the gripper are a length of 50 mm, width of 20 mm, and thickness of 15 mm. The gripper's inner face is curved and tilts at an angle of 79.38 degrees (refer to Figure 3.21). In order for the gripper to hold the latex cup better and more steadily, the tilting angle is designed to match the angle of the latex cup design.

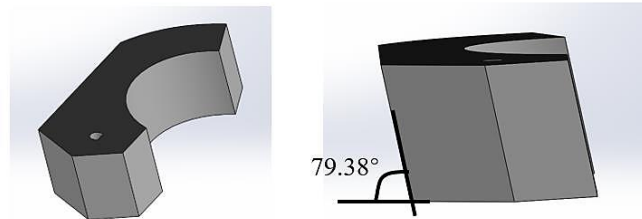


Figure 3.21: Gripper end-effector design

The gripper can simultaneously open and close by being driven by a motor to rotate two gears located on each side of the gripper. A motor holder was designed to be 50 mm long and 29 mm wide (refer to Figure 3.22). A gripper cover was designed to be 50 mm long and 29 mm wide and the motor holder will be placed on top of the gripper cover (refer to Figure 3.23). Small vents were designed on the motor holder to allow heat generated by the motor to escape.

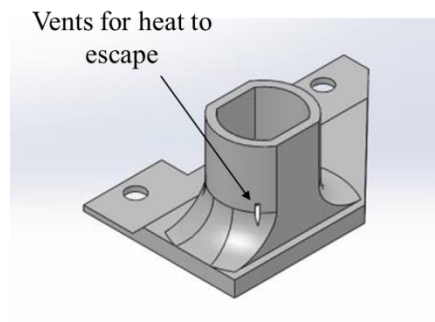


Figure 3.22: Motor holder design

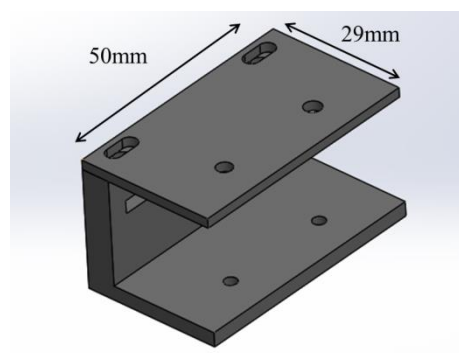


Figure 3.23: Gripper holder design

Two gear mechanisms were implemented in the gripper design to perform the pouring process. A small gear with 10 teeth was driven by a servo motor, and it will drive the large gear with 15 teeth. The big gear was then fastened to the gripper

holder and attached to the gripper support. This connection can allow rotation for the pouring process. Figure 3.24 shows the assembled parts of the gripping system.

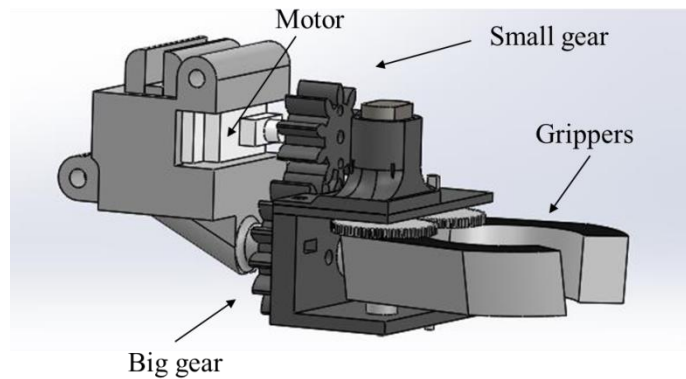


Figure 3.24: Gear mechanism that drives the gripper rotation

### 3.2.8 Storage Tank Design

The storage tank's external dimensions are length of 90 mm, width of 70 mm, and height of 27.5 mm. It is in a rectangular shape (refer Figure 3.25). The height of the tank cannot be designed with a large dimension since it will obstruct the manipulator's motion. To make pouring easier, the funnel and pipe were placed in the centre of the tank. The design of the pipe and funnel also prevents overflowing and spilling of the latex onto the robot.

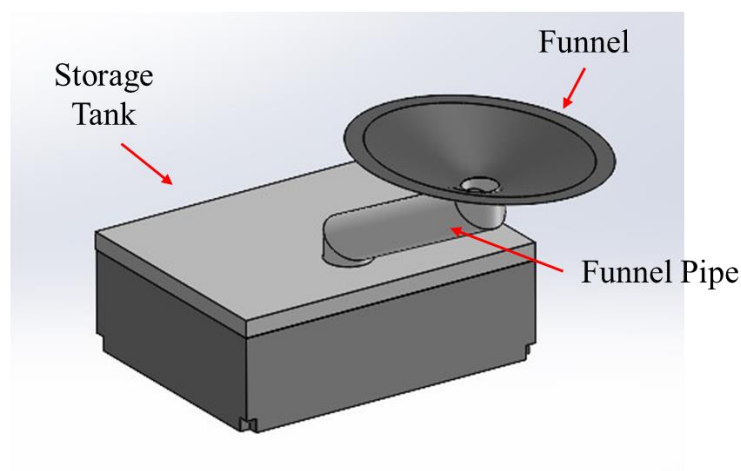


Figure 3.25: Storage tank, pipe and funnel design

The formula below can be used to calculate the maximum amount of liquid that this storage tank can hold, which is up to 104832 mm<sup>3</sup> or 104.832 ml of liquid:

$$V_{it} = W_{it} \times L_{it} \times H_{it} \quad (3.1)$$

where

$V_{it}$  = inner tank volume, mm<sup>3</sup>

$W_{it}$  = inner tank width, mm

$L_{it}$  = inner tank length, mm

$H_{it}$  = inner tank height, mm

In order to allow for easier removal of the latex from the storage tank, the robot platform was designed to be detachable. Four male slots and four female slots were created for the robot platform and storage tank, respectively (refer to Figure 3.26). This can allow the storage tank to be fixed in place when the robot is travelling.

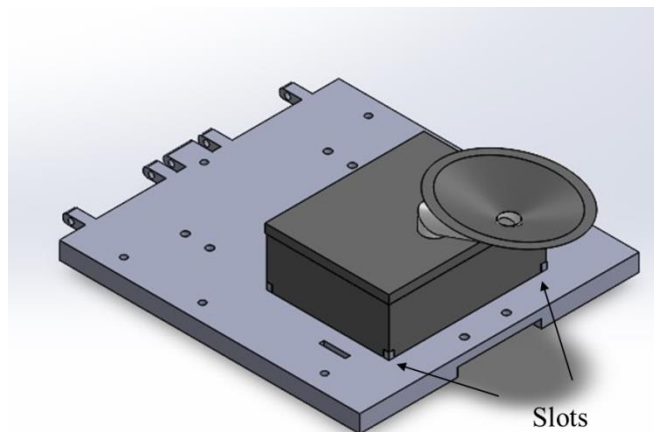


Figure 3.26: Fitting of storage tank into the robot platform's slots

When all of the robot's elements are positioned on the platform, the stress imposed on the platform increases. Therefore, the robot platform's bottom was reinforced to make it stronger and less likely to bend readily. The reinforcing design of the robot platform is depicted in Figure 3.27.

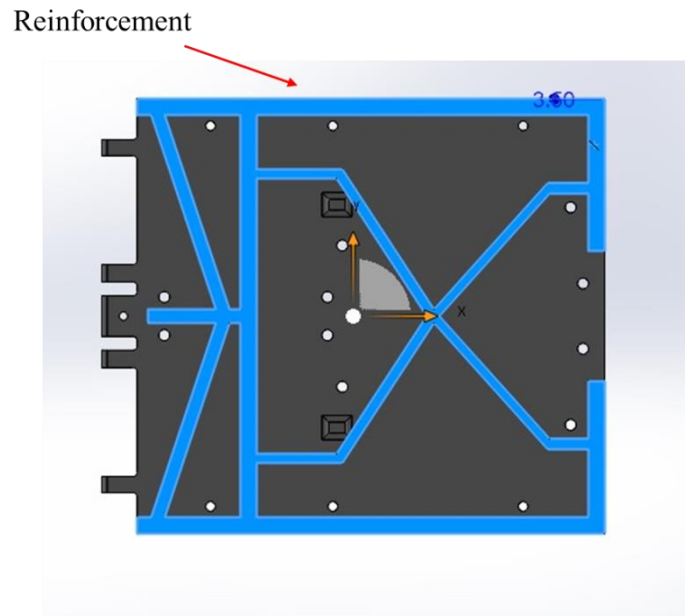


Figure 3.27: Reinforcing design at bottom of the robot platform

### 3.2.9 Encoder sensor holder

The encoder sensor holder was designed to hold the encoder sensor in position so that it can operate. An encoder sensor was located at the rotational base to detect the angle of rotation of the base with horizontal movement (refer to Figure 3.28). This could improve the accuracy of the robotic arm's rotation to the desired position to collect latex cups.

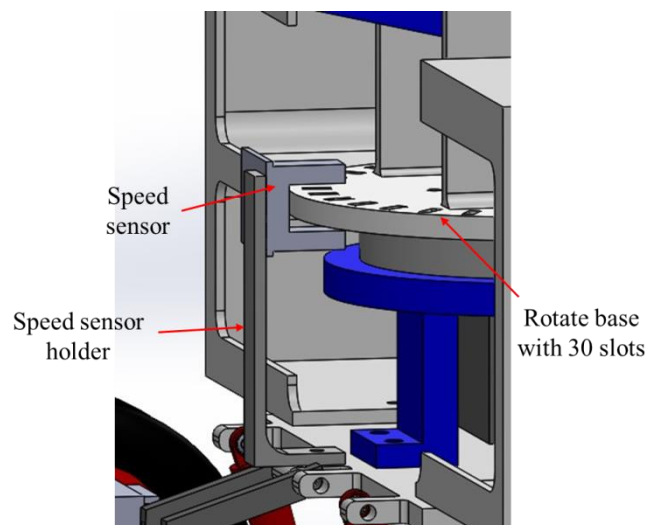


Figure 3.28: Encoder sensor holder for base with horizontal movement

### 3.2.10 Electronic components holder

In order to keep the electronic components from becoming wet, the holder was made to be an enclosed box. The electronic component holders were designed with a slot at the back to allow the controller board and other electronic components to connect to the power supply and wiring (refer to Figure 3.29). One of the electronic component holders was designed with two layers to store the electronic components (refer to Figure 3.30).

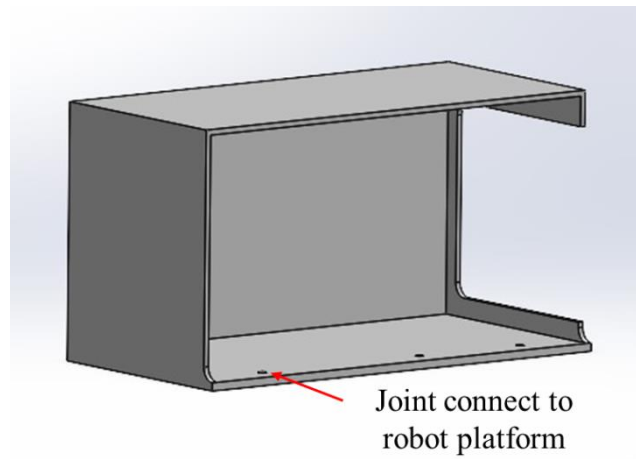


Figure 3.29: Electronic components holder with slot

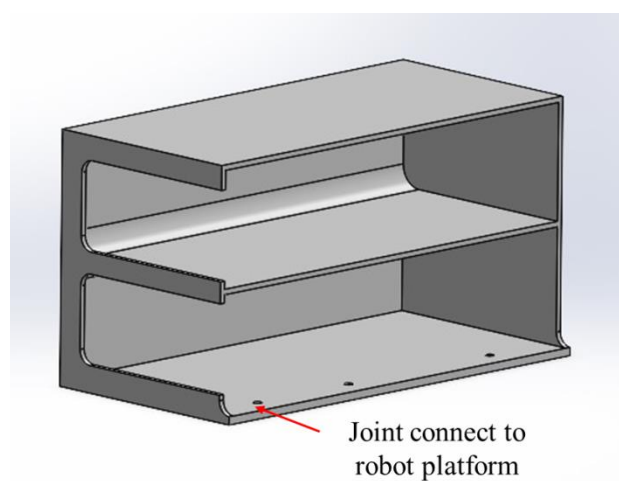


Figure 3.30: Electronic components holder with double layer

### 3.2.11 Base Storage Compartment

Last but not least, a container was created to house the battery, the steer-used DC motor that used to control the steering, and the 12V DC motor that used to power the motion of the robot prototype. With bolts and nuts, this compartment was fastened to the robot platform (see Figure 3.31).

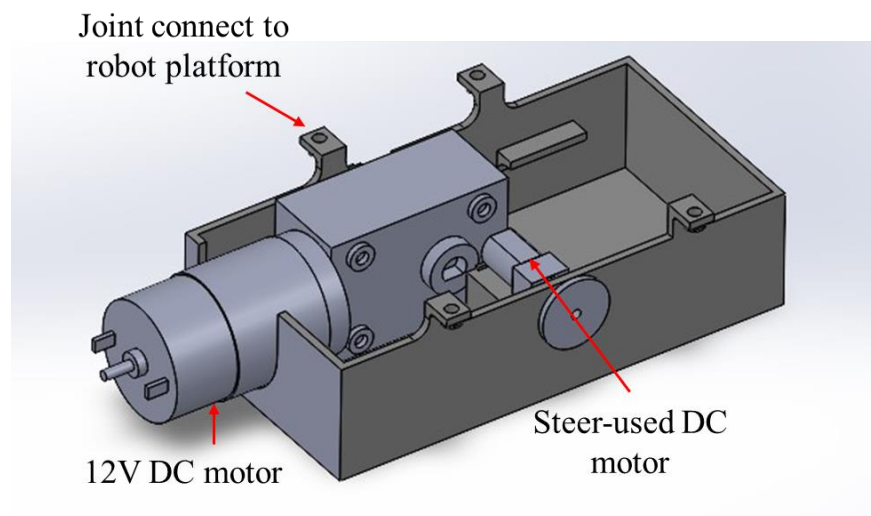


Figure 3.31: Base storage compartment for DC motor

### 3.2.12 Solidworks Assembly

An overall prototype design will be developed through the combination of the sub-function designs. The finished prototype design was then run through a variety of simulations to assess its viability before being built for a real-world trial.

#### 3.2.12.1 Mobility components

The locomotion and steering systems are combined and connected to the robot platform after all of their individual sub-functions have been designed. The

locomotion and steering systems have a width and length of 290.00 mm and 303.14 mm, respectively. The isometric perspective of the entire mobility subsystem is seen in Figure 3.32.

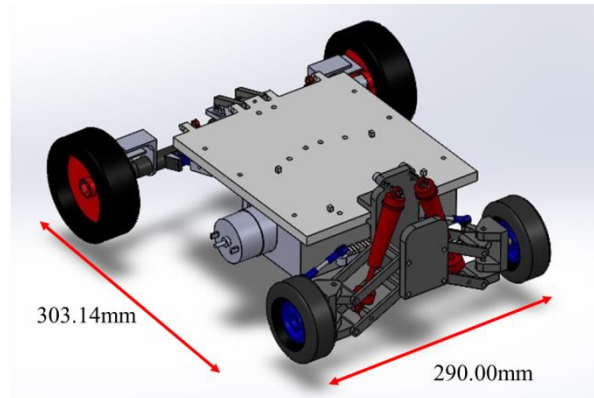


Figure 3.32: Mobility subsystem (Isometric view)

### 3.2.12.2 Manipulation components

All the parts of the manipulators and end-effector were connected using various diameters of threaded rod and self-locking nuts. The manipulation system in the Solidworks software is illustrated in Figure 3.33.

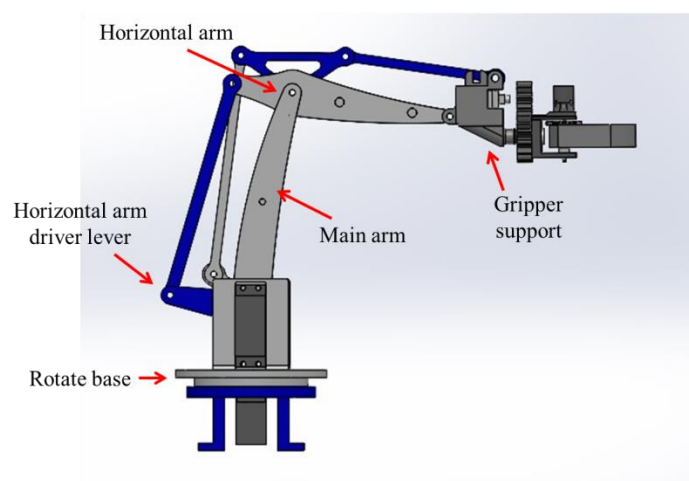


Figure 3.33: Assembly of manipulation components

### 3.2.12.3 Overall Assembly

The entire prototype assembly is completed by joining the mobility component, manipulation component, and other components (refer to Figure 3.34). The Solidworks prototype measures a length of 303.14 mm, width of 290 mm, and height of 324.04 mm. The robot prototype has a weight of 2379.691 grammes.

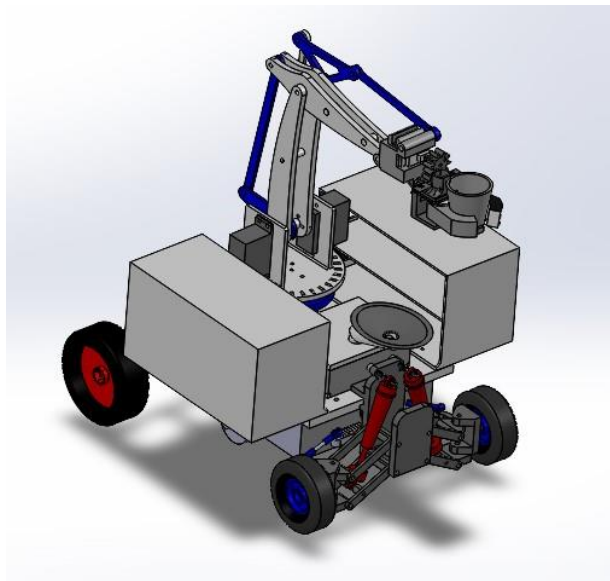


Figure 3.34: The latex cup robot collector's overall prototype design

## 3.3 Firmware configuration

To make sure the robot can operate properly, firmware consideration is a crucial responsibility. The components to be considered in the robot prototype are servo motors that are used to control the manipulation and DC motors that are used to control the mobility of the robot. The firmware options with their specifications and functionality for this robot are listed in Table 3.2 below.

Table 3.2: Firmware configuration and specification

Firmware options	Functionality	Specification
<p>1. A58SW-555 12V DC motor</p> 	<p>Mobility: Move the entire robot via using differential gear to transfer rotational motion to linear motion.</p>	<ul style="list-style-type: none"> <li>• Operating Voltage: 12 V</li> <li>• Operating Speed: 260 RPM</li> <li>• Rated Current: 2 A</li> <li>• Rated Torque: 9 kg.cm (SGrobot, n.d.)</li> </ul>
<p>2. Cytron 6V 85RPM DC motor</p> 	<p>1. Manipulation: Control the rotation of the gripper to grasp latex cups.</p> <p>2. Mobility: Use to rotate the gear and rack to control the steering the front wheels</p>	<ul style="list-style-type: none"> <li>• Operating Voltage: 6 V</li> <li>• Operating Speed: 85 RPM</li> <li>• Rated Current: 0.04 A</li> <li>• Rated Torque: 2 kg.cm</li> </ul>
<p>3. MG995 Servo Motor</p> 	<p>1. Manipulation: Control the main arm movement of the robotic arm.</p> <p>2. Manipulation: Control the horizontal arm movement of the robotic arm.</p> <p>3. Manipulation: Control the base movement of the robotic arm</p>	<ul style="list-style-type: none"> <li>• Operating Voltage: 4.8 -7.2 V</li> <li>• Operating Speed: 60 RPM</li> <li>• Rotation Angle: 0 - 180° for main arm and horizontal arm movement, 0 - 360° for base movement</li> <li>• Rated Current: 0.35 A</li> <li>• Rated Torque: 9 kg.cm</li> </ul>
<p>4. MG90S Servo Motor</p> 	<p>1. Manipulation: Control the rotation of the entire gripper to perform pouring process.</p>	<ul style="list-style-type: none"> <li>• Operating Voltage: 4.2 – 6 V</li> <li>• Rotation Angle: 0 – 180 °</li> <li>• Rated Torque: 1.5 kg.cm</li> <li>• Operating Speed: 0.3 sec / 60 °</li> </ul>

### 3.3.1 Parameter calculation

The applicability of these motors for the robot is determined by performing parametric calculations after obtaining the motor's specifications.

#### 3.3.1.1 Motor for robot transmission

When a robot climbs up a slope from resting to full speed, the motor is going to require its maximal power to function, and the motor's size will be determined by the maximum energy (Neal, 2010). To illustrate the forces on the robot when it accelerates up an incline, a free-body diagram was created (refer to Figure 3.35).

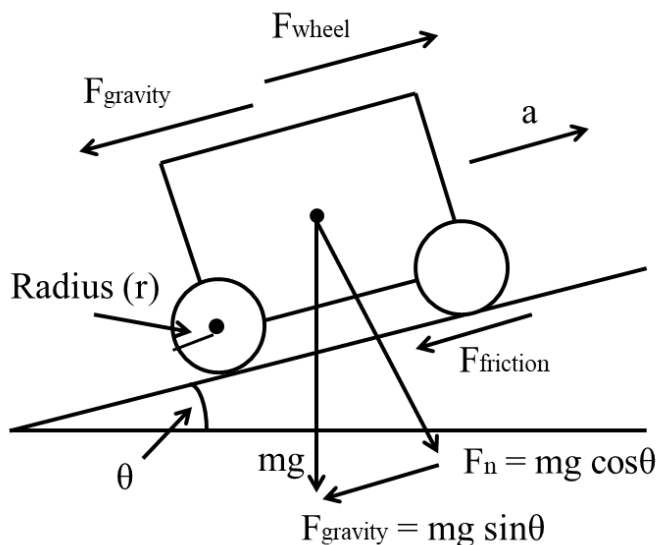


Figure 3.35: A free-body diagram of robot on an inclined terrain with slope  $\theta$

Some settings are specified before beginning:

- Robot's initial speed,  $v_o = 0$  m/s
- Robot's maximum speed,  $v_{max} = 0.1$  m/s
- Maximum incline slope to travel,  $\theta_{slope} = 30^\circ$
- Time for the robot from rest to reach maximum speed,  $t_a = 2$  sec

To make the calculations easier, frictional force was assumed to be omitted. The following equation was used to determine acceleration:

$$a = \frac{v_{max} - v_o}{t_a} \quad (3.2)$$

Where

$a$  = Robot's acceleration, m/s<sup>2</sup>

$v_{max}$  = Robot's maximum speed, m/s

$v_o$  = Robot's initial speed (rest), m/s

$t_a$  = Time for the robot from rest to reach maximum speed, s

The acceleration calculated was 0.05 m/s<sup>2</sup>.

The following equation was used to determine the lowest output torque necessary for turning the wheels by using calculated acceleration, a:

$$\rightarrow \Sigma F = m_{robot} \cdot a \quad (3.3)$$

$$(f_{wheel} - f_{gravity}) = m_{robot} \cdot a \quad (3.4)$$

$$f_{wheel} = (m_{robot} \cdot a) + f_{gravity} \quad (3.5)$$

$$f_{wheel} = (m_{robot} \cdot a) + (m_{robot} \cdot g \cdot \sin\theta_{slope}) \quad (3.6)$$

$$f_{wheel} = \tau / r \quad (3.7)$$

$$\tau = f_{wheel} \times r \quad (3.8)$$

Where

$m_{robot}$  = Mass of robot, kg

$f_{wheel}$  = Force exerted on the wheel, N

$f_{gravity}$  = Gravitational force acting on the robot on an incline, N

$a$  = Acceleration of robot, m/s<sup>2</sup>

$\theta_{slope}$  = Maximum incline slope to travel, °

$\tau$  = Torque, N·m

$r$  = Radius of the rear wheel, m

The torque obtained was 0.501 N·m. However, there is a gear ratio in the motor which is 2.5. The minimum input torque was calculated using the formula below:

$$\tau_{input} = \tau_{output} / \text{Gear ratio} \quad (3.9)$$

Where

$\tau_{input}$  = Input motor torque to power the differential gear, N·m

$\tau_{output}$  = Output motor torque for the rear wheels to drive the robot, N·m

The input torque obtained was 0.200 N·m, which is equivalent to 2.04 kg.cm.

Then, the maximum speed of the robot,  $v_{max}$ , which was previously determined, was used to calculate how fast the motor needed to spin. The following equation was used to determine the motor's speed:

$$RPM_{output} = \frac{v_{max}}{2\pi \times r} \quad (3.10)$$

$$RPM_{input} = \text{gear ratio} \times RPM_{output} \quad (3.11)$$

Where

$v_{max}$  = Robot's maximum speed, m/min

$r$  = Radius of rear wheel, m

$RPM_{input}$  = Motor's input rotational speed to power the differential gear, rev/min

$RPM_{output}$  = Motor's output rotational speed for the rear wheels to drive the robot, rev/min

The input rotational speed of the motor obtained was 56.17 RPM.

As a result, the A58SW-555 12V DC motor in Table 3.2 above was chosen since both the torque required and the speed required fall within the motor's specification. The robot requires a minimum torque of 2.04 kg.cm and a speed of 56.17 RPM.

### 3.3.1.2 Motor for robotic arm

To ascertain the operating torque needed to control the movement of the robotic arm, the main arm was examined. The torque applied to the main arm must not surpass the motor's stall torque; if the torque exceeds the stall motor torque, the motor will lose its ability to support the arm and it will drop. The torque is generated by forces exerted on the main arm, as displayed in Figure 3.36 below. The mass of the main arm is represented by  $F_A$ , while the remaining components attached after the main arm are represented by  $F_B$ .

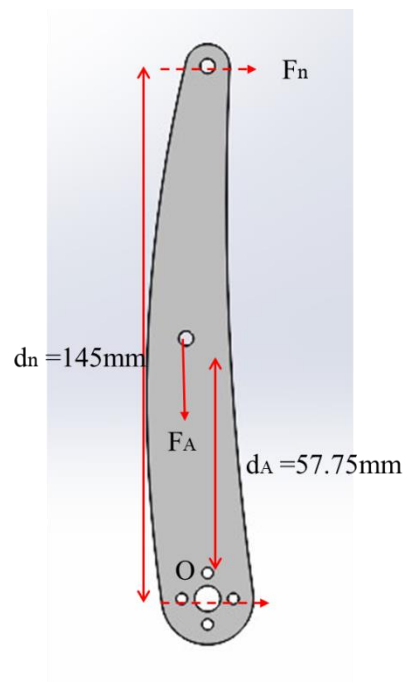


Figure 3.36: Forces exerted perpendicular to point O of the main arm

The following formula was used to calculate the torque acting on point O,  $\tau_o$ :

$$+ccw \tau_o = \Sigma F_n \times d_n \quad (3.12)$$

Where

$F_n$  = Force acting perpendicular to point O, where n = A and B, N

$d_n$  = Distance between force  $F_n$  and point O, where n = A and B, mm

The torque calculated was 0.345 N·m, or 3.618 kg.cm.

As a result, the MG995 servo motor is appropriate to control the motion of the main arm, as the obtained  $\tau_o$  was 3.618 kg·cm where the stall torque of the MG995 servo motor is 9 kg·cm which is greater than the required torque. It is proven that the MG995 will be able to hold main arm in position. The horizontal arm will also be controlled by the MG995 servo motor. Therefore, no calculations were conducted, as it will be able to function as the main arm will experience more torque than the horizontal arm.

### 3.3.1.3 Motor for gripper rotation (Pouring)

The mass moment of inertia was taken into account while calculating the torque required rotating the gripper because the pouring process requires angular movement. Parts A, B, and C make up the three independent parts of the gripper set (Figure 3.37). The mass moment of inertia was calculated using the Solidworks software. The angular velocity,  $\omega$  for the pouring process in Solidworks software was set 8 rev/min for 2 seconds. To simplify the calculation, the following formula was used to convert angular velocity to rad/sec:

$$\omega \text{ (rad / s)} = \omega \text{ (rpm)} \times \frac{2\pi}{60} \quad (3.13)$$

Where

$\omega$  = angular velocity, rad/s

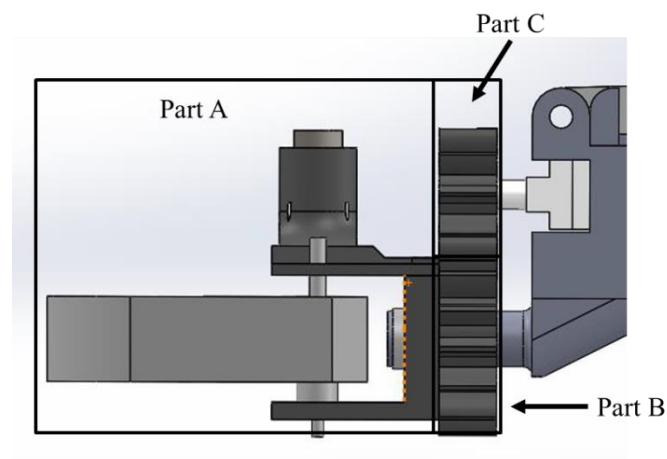


Figure 3.37: 3 separated parts of gripper set

Part A and part B are mounted together and will rotate together. The total inertia required to spin these two sections is determined by combining the mass moments of inertia for each component. Using the equation, the torque required to spin parts A and B was computed:

$$\tau_{part\ 1\ \&\ 2} = I_{part\ 1\ \&\ 2} \alpha = I_{part\ 1\ \&\ 2} (\omega/t) \quad (3.14)$$

Where

$\tau_{part\ 1\ \&\ 2}$  = Torque required rotating part 1 and 2, N·m

$I_{part\ 1\ \&\ 2}$  = Mass moment of inertia of part 1 and 2, kg·m<sup>2</sup>

$t$  = Time, s

$\alpha$  = Angular acceleration, rad/s<sup>2</sup>

Upon finding the torque required to rotate parts A and B, the torque was used to compute the torque needed to rotate part C. The following formula is used to determine the gear ratio:

$$\text{Gear ratio, } GR = \frac{\text{GearTeethdriven}}{\text{GearTeethdriving}} \quad (3.15)$$

The following formula is used to determine the torque needed for part C:

$$\tau_{part\ 3} = I_{part\ 3} \left( \frac{\omega(GR)}{t} \right) + \frac{(\tau_{part\ 1\ and\ 2})}{GR} \quad (3.16)$$

The motor torque needed for the gripper to perform pouring process is  $5.94 \times 10^{-6}$  N·m, or  $6.06 \times 10^{-5}$  kg·cm. The motor chosen is an MG90s with a 1.5 kg·cm rated torque. It proves that the motor is suitable to control the gripper, as the rated torque is sufficient to control the gripper.

### 3.4 Static Analysis

The robot prototype designed underwent to make sure that it could be built and joined together without breaking down. A computer programme named Finite Element Analysis (FEA) was utilised to compute the impacts of constant forces acting on the prototype's mechanical structure. The components that needed the perform FEA analysis using Solidworks software are the robot platform and robotic arm, as they will be experiencing the largest load in the prototype and may have the likelihood to break. The weight of the components was determined before undergoing the FEA analysis. The parts that will be fabricated using a 3D printer were set to PLA materials to ensure the accuracy of the analysis. Other parts such as motors were determined by weight balance. After getting the weight of the components, the following formula was used to convert the unit of the components from kg to Newton:

$$W_c = m_c \times g \quad (3.17)$$

Where

$W_c$  = Weight of component, N

$m_c$  = Mass of component, kg

$g$  = Gravity, m/s<sup>2</sup>

#### 3.4.1 Robot Platform

The first part to undergo FEA analysis is the robot platform. The component of the prototype that will be subject to the greatest loads is the robot platform. Electronic parts, a robotic arm, and a storage tank will all be positioned on top of the robot platform. The components that will be placed at the bottom of the platform are the base storage compartment for the DC motor and batteries. The positions of the components were shown in Figure 3.38. Table 3.3 below lists the weights and forces each component exerts on the robot platform.

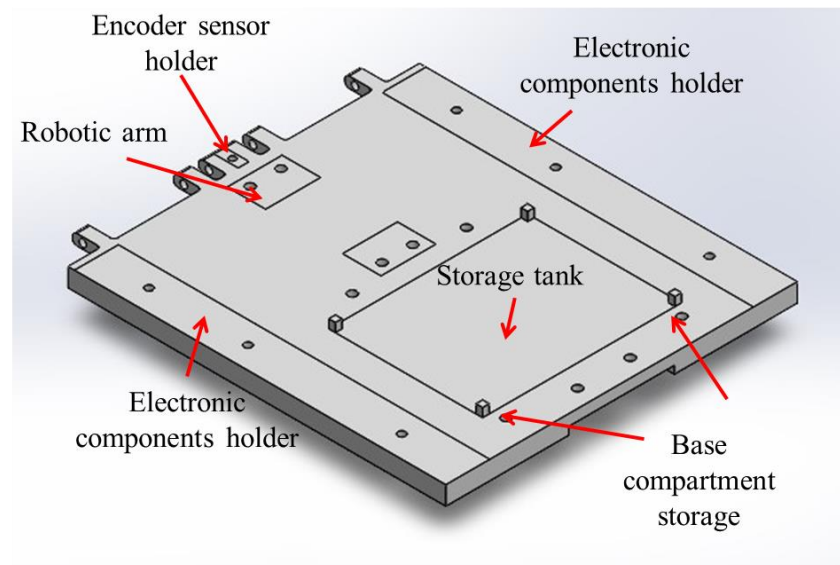


Figure 3.38: Position of components on the robot platform (top & bottom)

Table 3.3: Forces exerted on the robot platform

Components	Weight (g)		Force (N)
Storage tank filled with water	118.00 (storage tank) + 102.10 (water)	210.00	2.06
Electronic storage (Left)	152.30 (storage) + 150 (chip)	302.30	2.97
Electronic storage (Right)	124.40 (storage) + 120.713 (chip)	245.113	2.40
Base storage compartment	69.50 (storage) + 10 (5V DC motor) + 126 (battery) + 428 (12V DC motor)	633.50	6.21
Encoder sensor holder	1.90 (holder) + 2.456 (encoder)	4.356	0.04

The robotic arm has a weight of 0.433 kg. Since the robotic arm will extend and retract while carrying out the latex cup collecting operation, it is necessary to determine the force that the robotic arm will apply to the robot platform independently. The robot platform will experience compression and tension as the robotic arm extends since its centre of mass is outside the base's designated area, which is indicated by the red line in Figure 3.39. Figure 3.39 shows a simplified free body diagram of the robotic arm under extended conditions (critical conditions). The distances shown are the distances between Point A and the centres of mass of the components. Then, the weight of parts of the robotic arm is shown in Table 3.4 below.

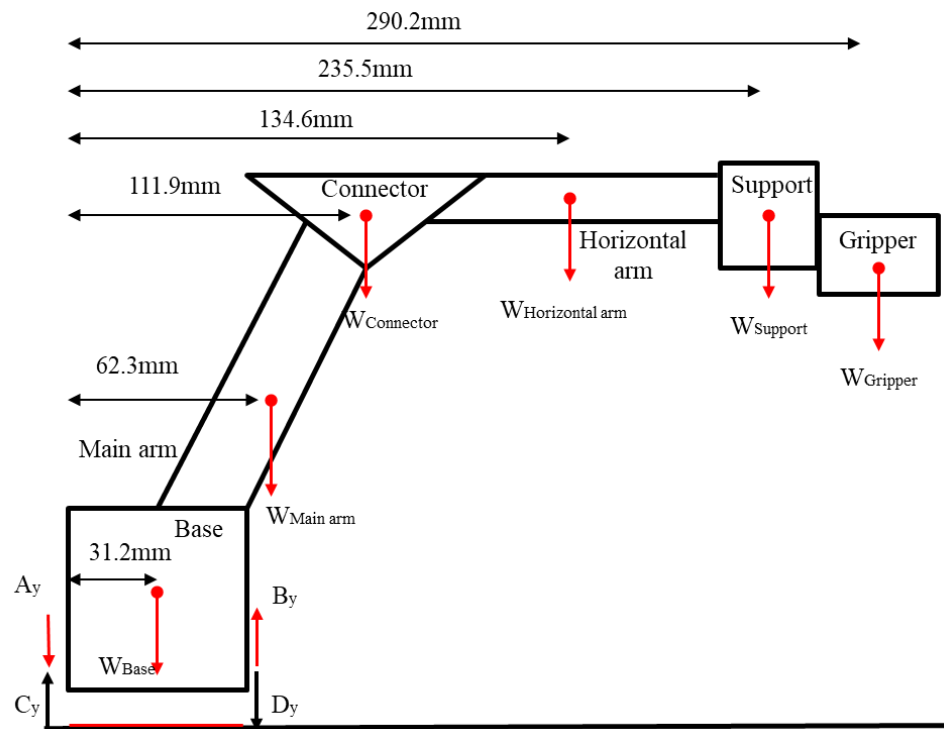


Figure 3.39: Simplified free body diagram of extended robotic arm

Table 3.4: Weight of each components of robotic arm

Components	Weight (g)		Force (N)
Base	27.10 (fixed base) + 46.20 (rotation base) + 20.2 (outer support) + 55.0 *3 (MG995 servo motor)	258.50	2.54
Main arm	13.50 (printed parts) + 14.80 (printed parts)	28.30	0.28
Connector	4.00 (printed part)	4.00	0.04
Horizontal arm	13.10 (printed parts) + 14.00 (printed parts)	27.10	0.27
Support	35.40 (printed part) + 13.40 (MG90S servo motor)	48.80	0.48
Gripper (With latex cup)	25.00 (printed parts) + 16.00 (gripper parts) + 35.50 (latex cup filled with water)	66.50	0.65

The equilibrium equation was used to determine the forces the robotic arm applied to the platform after all the necessary data and parameters had been accumulated:

$$+ \uparrow \Sigma F_y = 0 \quad (3.18)$$

$$- A_y - W_{base} + B_y - W_{Main\ arm} - W_{Connector} - W_{Horizontal\ arm} - W_{support} - W_{Gripper} = 0 \quad (3.19)$$

$$+ cw \Sigma M_A = 0 \quad (3.20)$$

$$W_{Base}(31.2) - B_y(62.5) + W_{Main\ arm}(62.3) + W_{Connector}(111.9) + W_{Horizontal\ arm}(134.6) + W_{support}(235.5) + W_{Gripper}(290.2) = 0 \quad (3.21)$$

$$A_y = -C_y \quad (3.22)$$

$$B_y = -D_y \quad (3.23)$$

Where

$F_y$  = Forces acting at the Y direction, N

$V_y$  = Forces acting on point V in the Y direction, where V = A, B, C, and D, N

$M_A$  = Moment at point A, N·mm

The computed forces for  $C_y$  (tension) and  $D_y$  (compression) are 2.77 N and 7.03 N respectively.

In order to prevent deformation of other areas of the robot platform, fixtures were applied within the spline line area. A fixture hinge was applied to the connection between the rear wheels and the robot platform, as it will be screwed with shock dampers (refer to Figure 3.40).

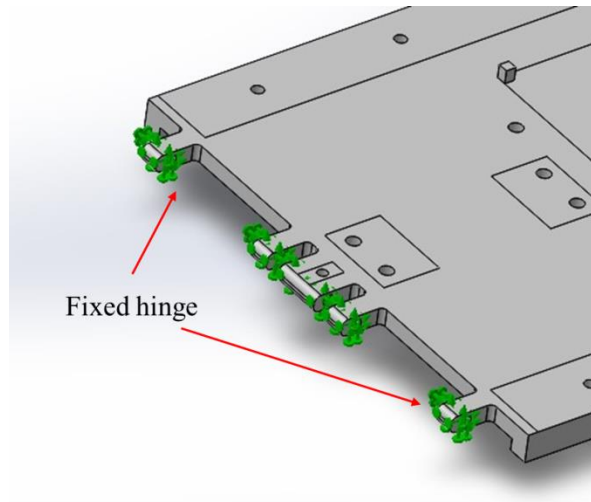


Figure 3.40: Fixture set on the robot platform

### 3.4.2 Robotic Arm

The robotic arm performed static analysis in extended state to identify the maximum stress, displacement and strain of the robotic arm. The external load acting on the robotic arm is the latex cup with water on the gripper. The load of a latex cup with water is 0.348 N. In order to undertake static analysis, fixtures were made to the robotic arm's base and pins were connected at each joint to keep the robotic arms linked. Figure 3.41 shows the static analysis of the robotic arm in Solidworks software.

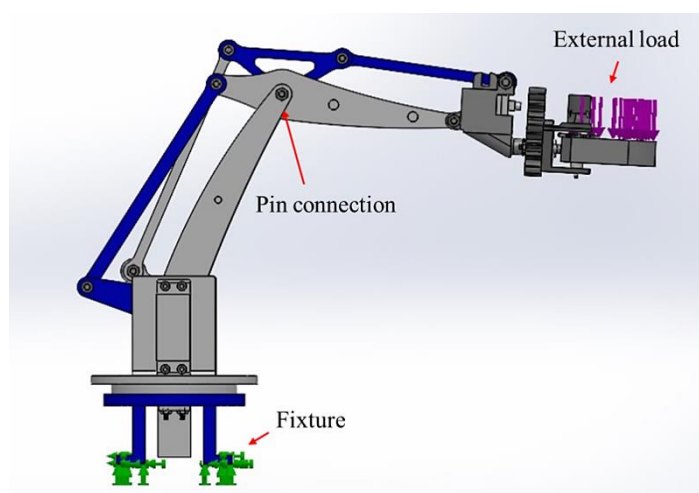


Figure 3.41: Static analysis of robotic arm Solidworks

### 3.5 Centre of mass: Toppling analysis

Toppling analysis was used to test the robot prototype's stability. The maximum slope angle the robot can function without tipping over can be determined via topple analysis.

#### 3.5.1 Centre of mass identification

A topple will occur when the centre of mass of the robot falls outside of the robot's footprint. Centre of mass of the robot for X, Y and Z direction was determined by using the formulas below:

$$x_{cg} = \frac{\sum_1^n m_n g x_n}{\sum_1^n m_n g} \quad (3.24)$$

$$y_{cg} = \frac{\sum_1^n m_n g y_n}{\sum_1^n m_n g} \quad (3.25)$$

$$z_{cg} = \frac{\sum_1^n m_n g z_n}{\sum_1^n m_n g} \quad (3.26)$$

Where

$n = 1, 2, 3 \dots, n$

$x_{cg}$  = Centre of gravity in X direction relative to a point, mm

$y_{cg}$  = Centre of gravity in Y direction relative to a point, mm

$z_{cg}$  = Centre of gravity in Z direction relative to a point, mm

$n$  = Number of parts

$m_n$  = Mass of parts, g

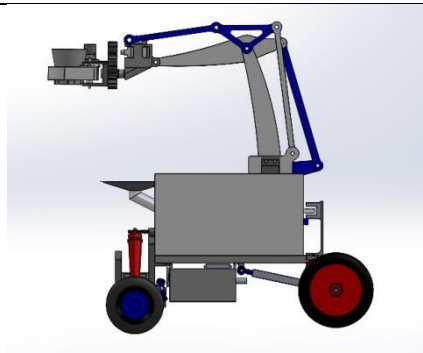
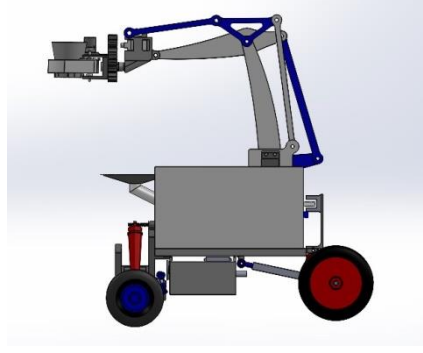
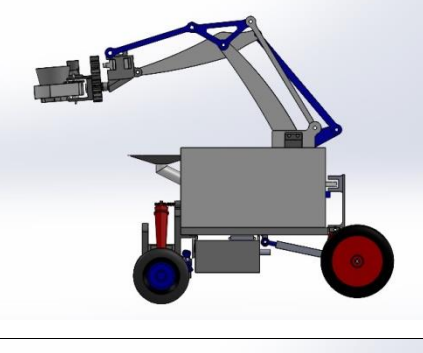
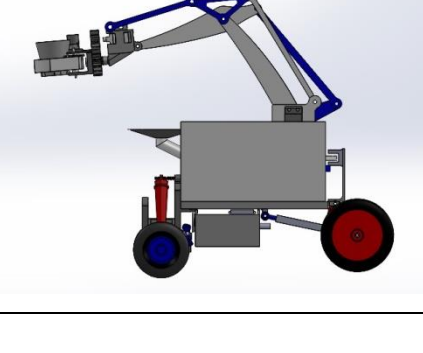
$x_n$  = Centre of gravity of that component n in X direction relative to a point, mm

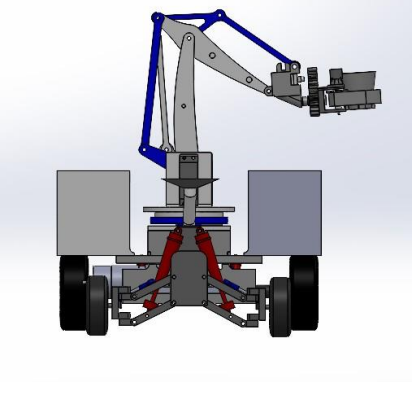
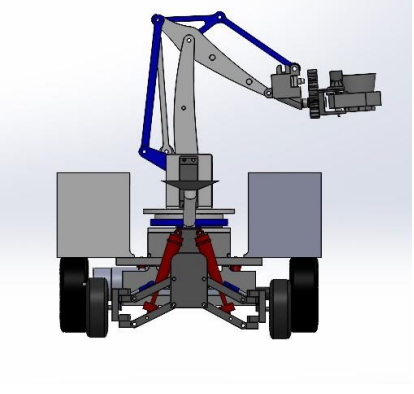
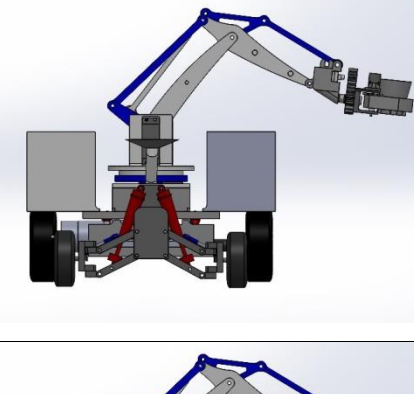
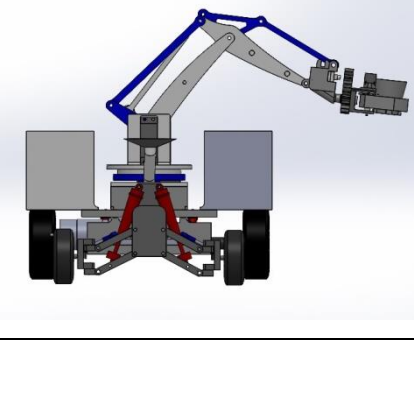
$y_n$  = Centre of gravity of that component n in Y direction relative to a point, mm

$z_n$  = Centre of gravity of that component n in Z direction relative to a point, mm

Solidworks software can be used to generate the centre of mass. Various positions of the robotic arm will have an impact on the position of the robot's centre of mass. When the robots extend, retract, and rotate, there are eight situations to choose from in order to pinpoint its centre of mass. Table 3.5.1.1 shows the eight situations for the robots.

Table 3.5: Eight centre of mass identification situations

Situation	Arm	Tank	Picture
1	Retracted	Empty	
2	Retracted	Full	
3	Extended	Empty	
4	Extended	Full	

5	Retracted	Empty	
6	Retracted	Full	
7	Extended	Empty	
8	Extended	Full	

### 3.5.2 Topple Angle

The centre of mass values was used to calculate the toppling angle. The front, rear, left, and right sides of the robot must be considered when calculating the toppling

angle for each situation. The toppling analysis can show whether the robot is capable of carrying out duties on uneven surfaces. The free body diagram of the robot with a left topple and a back topple is displayed in Figure 3.42. The toppling angle is determined using the following formulas:

$$\theta_{topple} = 90^\circ - \alpha \quad (3.27)$$

$$\alpha = \tan^{-1}\left(\frac{Y}{X}\right) \quad (3.28)$$

Where

$\theta_{topple}$  = Topple angle, °

$Y$  = Vertical distance of centre of mass from the floor, mm

$X$  = Horizontal distance of centre of mass from the robot side, mm

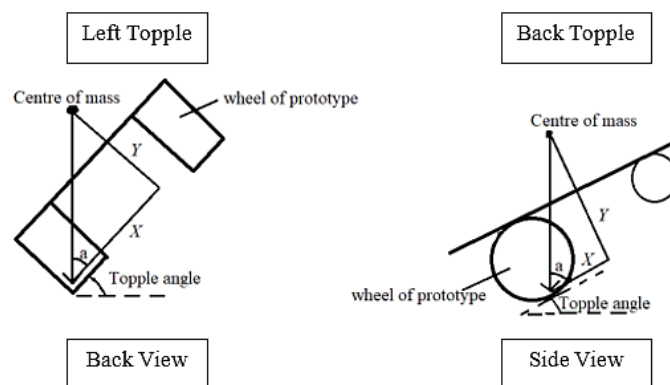


Figure 3.42: Left and back topple free body diagram

### 3.6 Motion Study

The dynamic behaviour of the robot's manoeuvrability when navigating across uneven ground was investigated via motion studies. To depict the scenario of uneven ground in the actual world, a basic, bumpy track with barriers was constructed. The barriers were made to be 10 mm tall with a 45 ° incline and 15 mm tall with a 50 ° gradient.

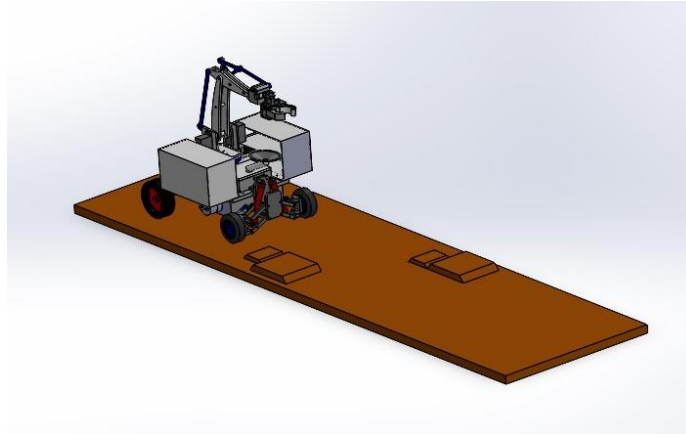


Figure 3.43: Uneven terrain created for Motion Study in Solidworks

The robot experiences a  $9806.65 \text{ mm/s}^2$  gravitational force on its Z-axis, which is pointing in the direction of the track.

### 3.6.1 Motor Feature

The parameters for the motor feature in Solidworks are displayed in Figure 3.44 below. The motor feature is applied to the rear wheel system and the speed of the wheels is set to be 51.67 RPM.

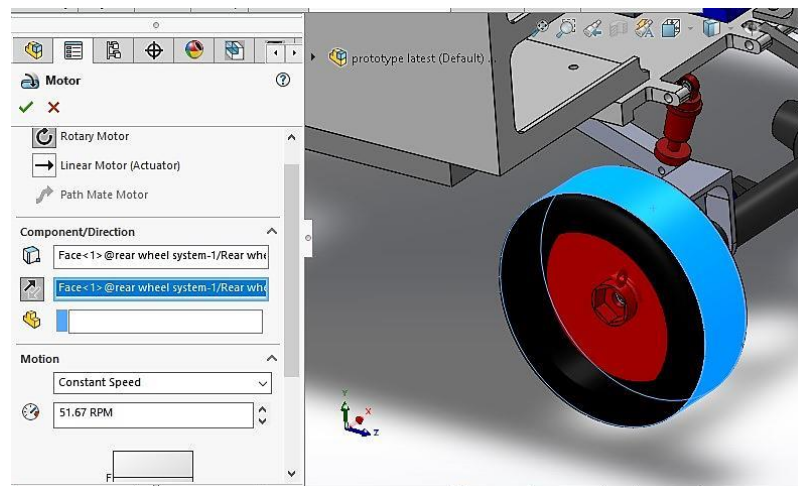


Figure 3.44: Motor feature setting in Solidworks

### 3.6.2 Spring Feature

The spring constant of the suspension system was applied using the spring feature in Solidworks. The spring constant of the front wheel system is 0.6258 N/mm while the spring constant of the rear wheel system is 0.1264 N/mm. The values for the spring constant were entered in the spring feature in the Solidworks motion study to conduct motion study analysis. Figure 3.46 and 3.46 illustrate the settings of the spring feature for the front wheel system and the rear wheel system, respectively.

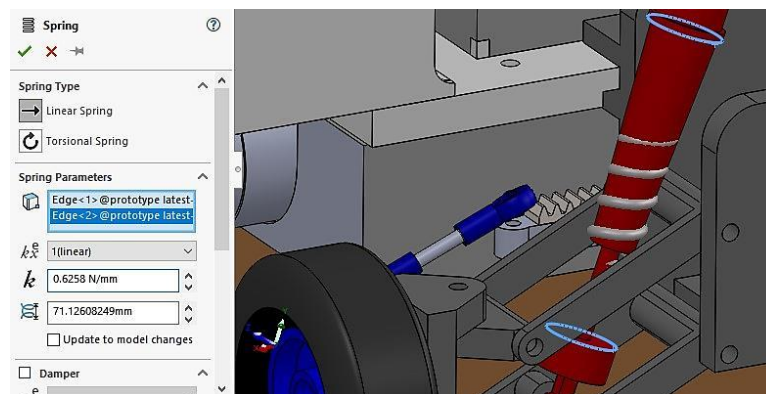


Figure 3.45: Spring feature of front wheel system in Solidworks

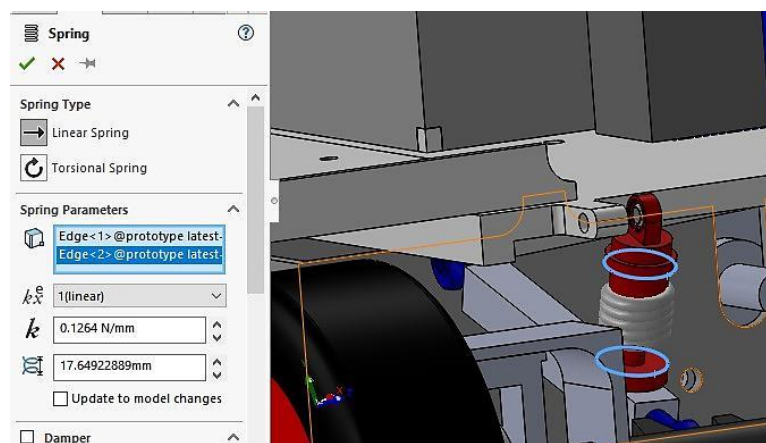


Figure 3.46: Spring feature of rear wheel system in Solidworks

### 3.6.3 Contact Feature

A friction coefficient will be added to the contact between robot wheels and track surfaces to obtain a better simulation result. According to Townsend (2002), the

kinematic friction and static friction on concrete surfaces have values of 0.8 and 1, respectively. Both of the values are included in the contact feature setting in Solidworks to perform motion study.

### **3.7 Fabrication of Prototype and Experiment Setup**

#### **3.7.1 Fabrication of Prototype**

The Raise3D N2 3D printer, located in the UTAR Industrial Engineering Lab, was used to build the designed component. The material used to fabricate the designed parts is PLA plastic. The 3D drawings will then be converted into stereolithography (STL) files to be opened in the slicing software named ideaMaker to edit the settings for 3D printing. The settings to be edited are infill pattern, infill density, thickness of layer, support and raft enablers. The STL files will then be converted to G-code files so that the 3D printer may build the designed components when the settings have been modified. The infill pattern used to fabricate the designed parts is grid pattern with an infill density of 10 % to 40 %, depending on the strength required for the designed parts to withstand the forces exerted on them.

#### **3.7.2 Experiment Setup**

This section will illustrate the experiment setup for topple angle test and prototype test run.

### 3.7.2.1 Setup for Topple Angle Test

To calculate the experimental topple angle and confirm the theoretical topple angle estimate for the robot prototype in Chapter 3.5.2, a topple test was conducted. An adjustable laptop stand was employed as the slope for the robot prototype to stand on, as shown in Figure 3.47. The laptop stand has seven different angles, which include 15 °, 21 °, 26 °, 32 °, 37 °, 41 ° and 45 °. The prototype will be placed on the laptop stand at the first angle. The angle of inclination increase gradually until the robot prototype toppled. Eight situations were planned for the toppling test, but only four of them were actually executed. The topple test was only carried out for four scenarios with empty an latex tank and latex cup to avoid an overflow of water that might damage the electronic components.



Figure 3.47: Laptop stand with adjustable height for topple angle testing

### 3.7.2.2 Setup for Prototype Test Run

1.5-litre water bottles served as the “rubber trees” with 300 mm between each bottle (Figure 3.48). The spacing between rubber trees is between 2.5 m and 3 m within a row (Sahuri, 2021). On a scale of 10, the water bottles were separated by 300 mm. The robotic arm's flexibility was then tested using latex cups that were placed at varied heights of 90 mm, 150 mm, and 190 mm (Figure 3.49). In order to contrast the motion study done in Chapter 3.6, barriers of 10 mm height with a 45 ° incline and 15 mm height with a 50 ° gradient were employed to assess the robot prototype's

capacity to traverse uneven terrain. Figure 3.50 shows the barriers arrangement for the robot prototype to travel across.

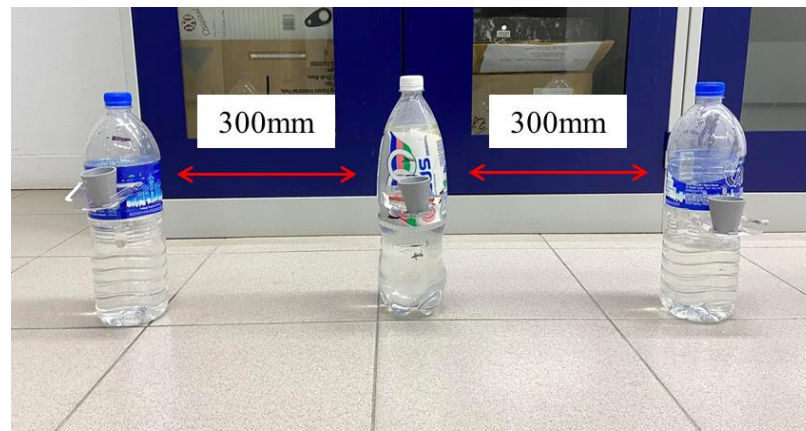


Figure 3.48: Rubber trees setup



Figure 3.49: Latex cups positioned at different heights

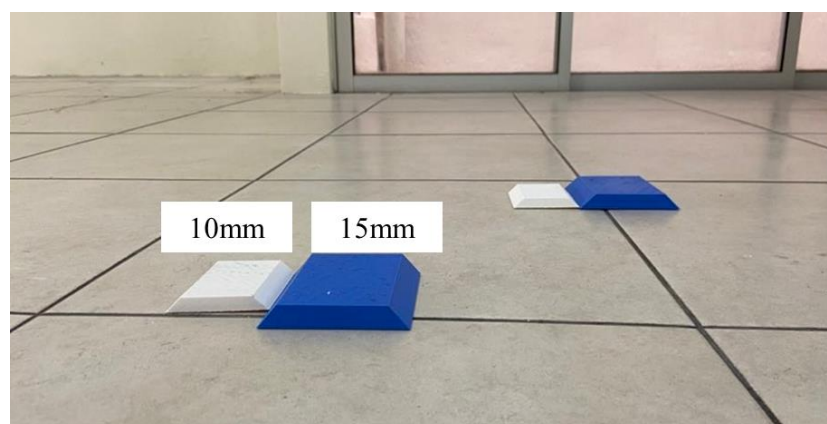


Figure 3.50: Barriers arrangement for mobility test

### 3.8 Project Planning and Milestone

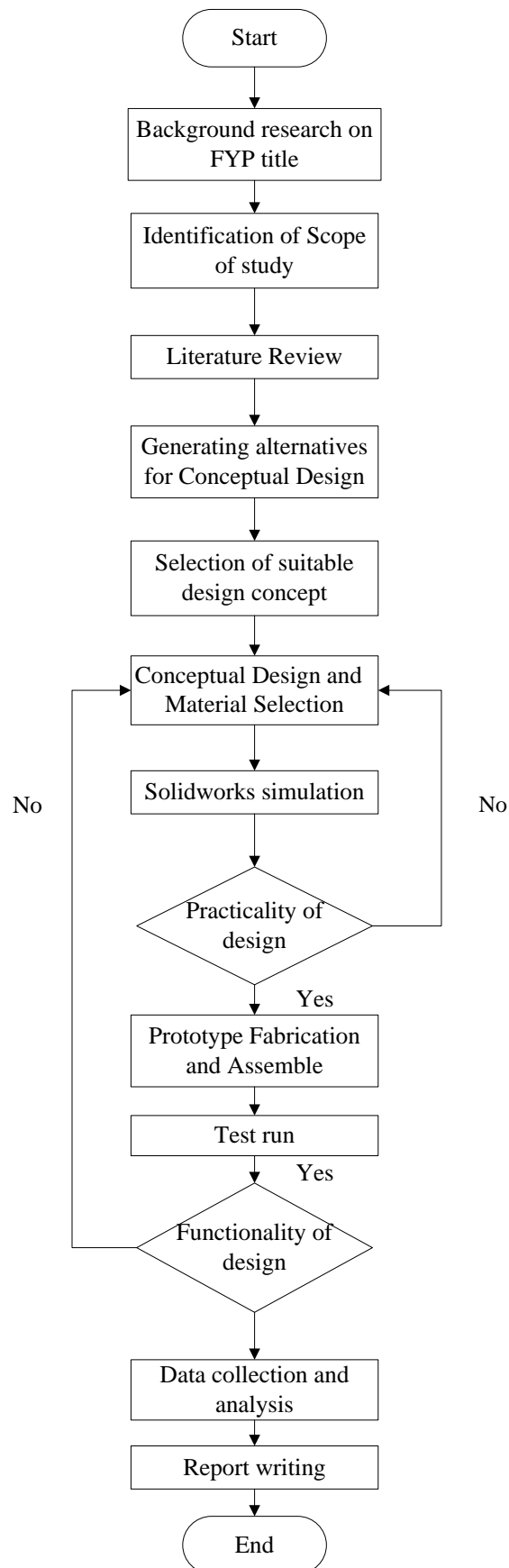


Figure 3.51: The project's overall flowchart

Figure 3.51 above depicts the project's workflow. To accomplish the entire study, it is separated into two stages, designated FYP 1 and FYP 2. This project will take a year to complete.

In FYP1, background research was conducted on the title of final year project to better understand the concept and determine the scope of study of the project. Next, a literature review of previous researchers was conducted to learn how to adapt and improve the design of the project. To select the most suitable design for the final conceptual design, various component design concept alternatives were created and considered. The design process was initiated using Solidworks software after selecting the final designs for each component. At the same time, appropriate materials and components that needed to be purchased were researched and selected so that the design was suitable to fit the dimensions of the components. Lastly, simulation is carried out after the completion of the prototype design.

In FYP2, simulations were conducted to check the feasibility of the design. Amendments could be made when the design is not feasible before fabricating the robot prototype. After the prototype is fabricated, the parts will be assembled. A test run was carried out to ensure the robot prototype is able to operate and perform tasks. If the prototype was not able to fulfil the scope of this project, calibration and modification of designs are required. Data collection for the experiments will be conducted after the final version of the robot prototype is developed. The data to be collected is the cycle time of the robot prototype to collect latex cups and topple angles. Lastly, the collected data will be analysed and report writing will continue to complete this project.

Below Gantt chart, Table 3.6 and 3.7 is used to determine the project planning schedule and keep track of the project's progress of FYP1 and FYP2.

Table 3.6: Gantt chart of FYP1

No.	Project Activities	W1	W2	W3	W4	W5	W6	W7	W8	W9	W10	W11	W12	W13	W14
1	Background research on FYP title														
2	Identification of scope of study														
3	Conduct literature review and generate alternatives for conceptual design														
4	Conceptual design and material selection														
5	Report writing														
6	Project presentation														
7	Simulation														

Planned  
 Actual

Table 3.7: Gantt chart of FYP2

No.	Project Activities	W1	W2	W3	W4	W5	W6	W7	W8	W9	W10	W11	W12	W13	W14
1	Simulation, prototype fabrication and assemble														
2	Trial run, calibration and modification														
3	Collect and analyse data														
4	Report Writing														
5	Project presentation														

Planned  
 Actual

## CHAPTER 4

### RESULTS AND DISCUSSIONS

#### 4.1 Latex Cup Collector Robot Prototype

3D-printed parts, electronic components and wire connection of the control system were assembled to build the latex cup collector robot prototype. The dimensions of the robot prototype are about 303 mm in length, 290 mm in width and 324 mm in height. The prototype weighed 2593 grammes and has 213.309 grammes difference from the weight obtained from Solidworks. The weight difference is due to the wires and fasteners used in the robot prototype, the weight difference may cause the experimental results to have a slight difference from the simulation results. Below are figures showing different views of the prototype for better illustration.

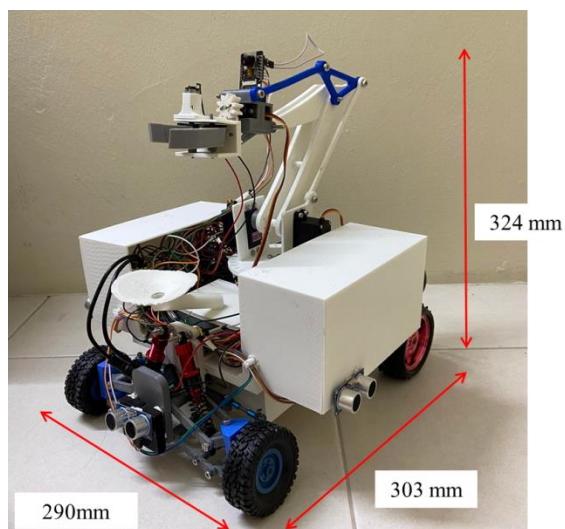


Figure 4.1: Latex Cup Collector Robot Prototype (Isometric View)

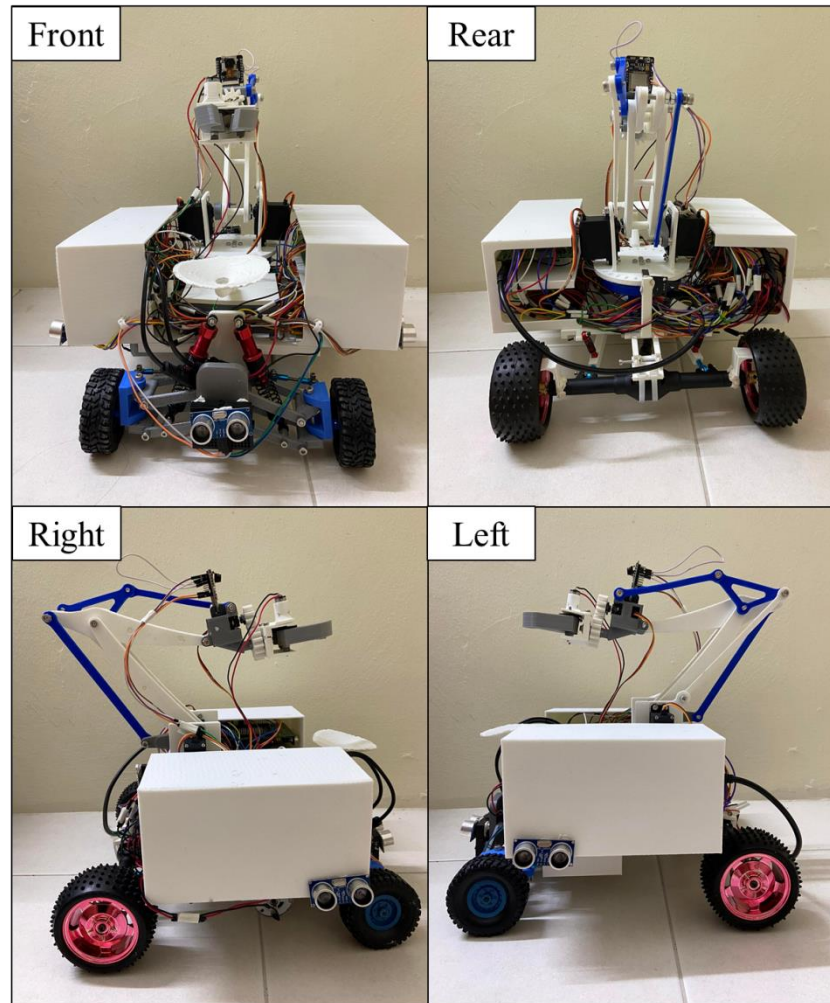


Figure 4.2: Latex Cup Collector Robot Prototype (front, rear, right and left view)

#### 4.2 Finite Element Analysis (Static test)

Three different types of plots—the stress plot, displacement plot, and strain plot—were obtained by Finite Element Analysis (FEA) simulation. The forces that are applied to the body and have a tendency to distort it are displayed using a stress plot. Moreover, a displacement plot is used to determine how much of the original position will distort. Lastly, the length of the deformed body changes is shown in a strain plot.

### 4.2.1 Robot Platform

In this part, the FEA results obtained for the simulation of the robot platform with an extended robotic arm will be discussed. The robot platform will experience maximum force applied to it when the robotic arm is extended.

Figure 4.3 shows the stress plot for the robot platform. The minimum stress experienced by the robot platform is  $1.166 \times 10^1 \text{ N/m}^2$ , while the maximum stress is  $4.240 \times 10^6 \text{ N/m}^2$ . The connection between the robot platform and robotic arm, which supports the entire weight of the extended robotic arm, is where the robot platform experiences the most stress. Another area of maximum stress exerted on the robot platform is the connection between the robot platform and the front wheel system. This is due to the weight of the extended arm increasing the force experienced by the front wheel system. The result obtained from the simulation is feasible as it does not exceed the yield strength of the PLA plastics of  $7.00 \times 10^7 \text{ N/m}^2$ .

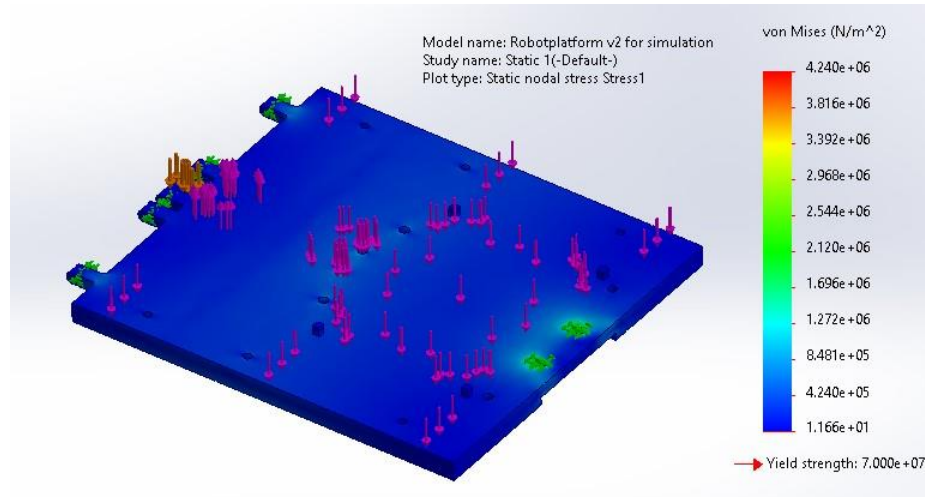


Figure 4.3: Stress plot for robot platform

The displacement plot for the robot platform is displayed in Figure 4.4. The maximum displacement determined from the simulation for the robot platform is  $1.275 \times 10^{-1} \text{ mm}$ . The red zone in Figure 4.2.1.2 shows the largest deformation experienced by the robot platform, which is on both sides of the robot platform. Both sides of the robot platform will experience the largest deformation as the electronic

components and compartments to store the electronic components contribute to the large force acting on the robot platform.

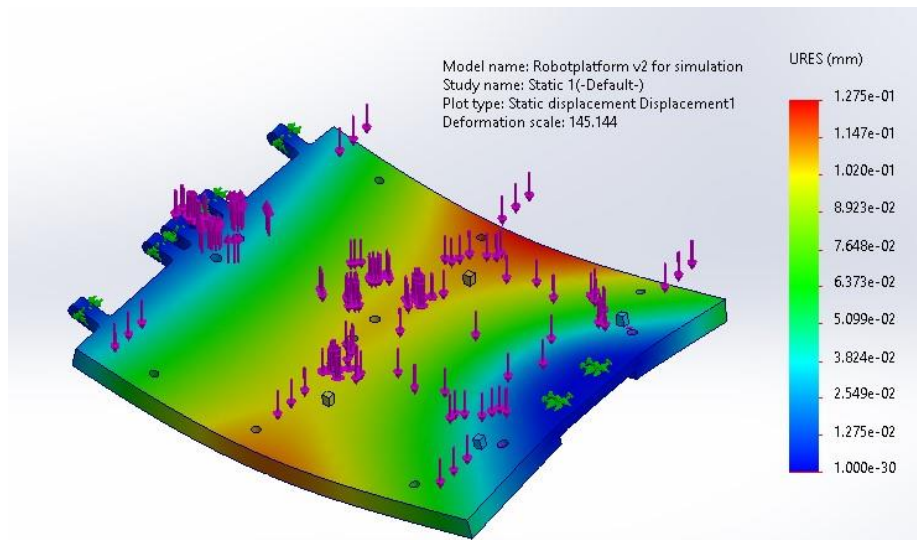


Figure 4.4: Displacement plot of robot platform

The robot platform's maximum strain is depicted in Figure 4.5. The positions where the robot platform connects to the robotic arm and the front wheel system are where the robot platform is subjected to the greatest strain. The maximum change in length to initial length ratio is  $7.068 \times 10^{-4}$  mm/mm. However, it does not cause any breakdown of the robot platform.

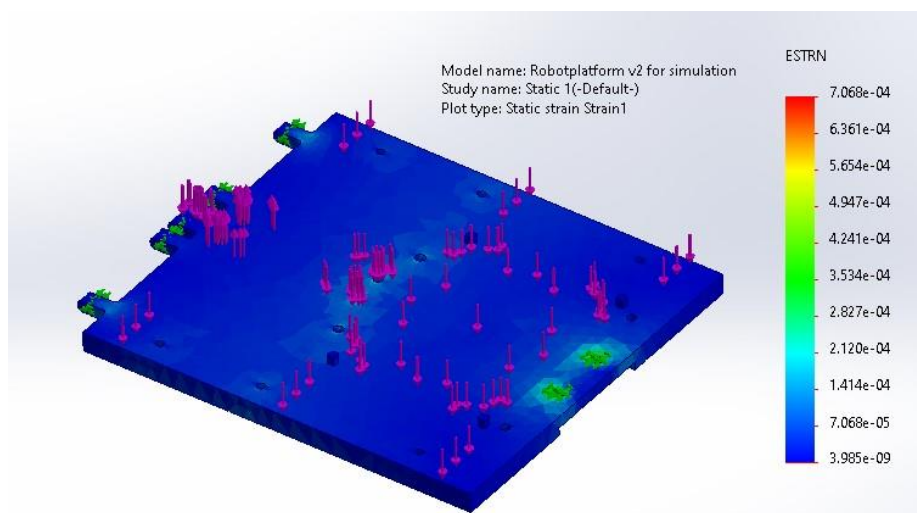


Figure 4.5: Strain plot of robot platform

### 4.2.2 Robotic Arm

The FEA simulation results for the robotic arm when it is extended will be explained in the following section. The robotic arm was extended for the simulation, as this is when it will be subjected to the most force.

In Figure 4.6, the maximum stress acting on the robotic arm is  $7.553 \times 10^6$  N/m<sup>2</sup>, whereas the minimum stress is 0.00 N/m<sup>2</sup>. The connection between the motor used to execute the pouring function and the gear attached to it puts the robotic arm under the greatest stress. Figure 4.7 displays the section view of the maximum stress exerted on the robotic arm. The result obtained from the simulation is feasible as it does not exceed the yield strength of the PLA plastics of  $7.00 \times 10^7$  N/m<sup>2</sup>.

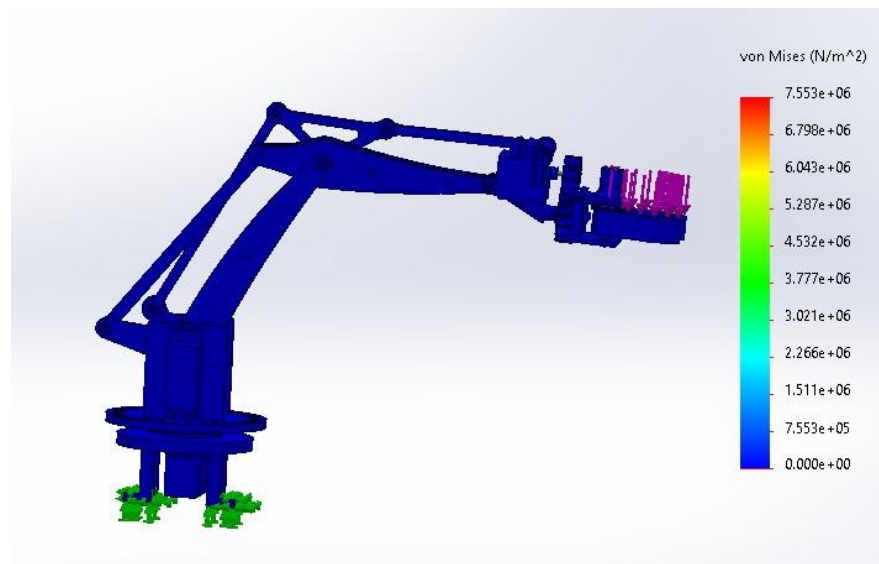


Figure 4.6: Stress plot of extended robotic arm

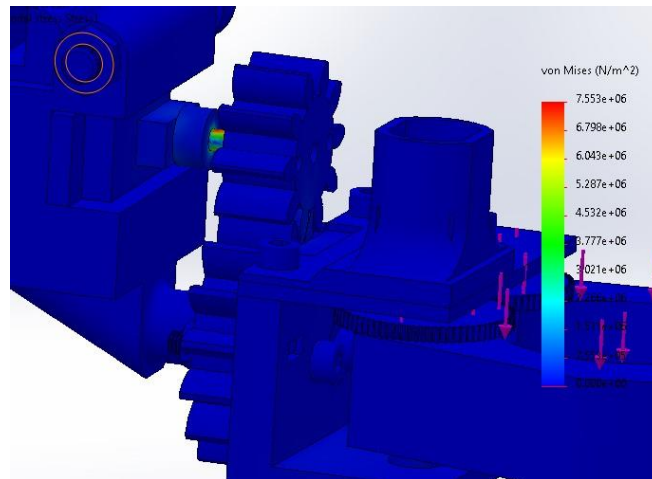


Figure 4.7: Stress plot of the gripper part (Section view)

Figure 4.8 shows the displacement plot of the extended robotic arm. The gripper end of the robotic arm has the largest displacement, with a value of  $7.391 \times 10^{-1}$  mm. This is due to the large weight of the gripper support, causing the gripper to displace from its original position. This also shows the result of maximum stress acting on the connection between the motor and the gear, which causes it to deform easily compared to other parts.

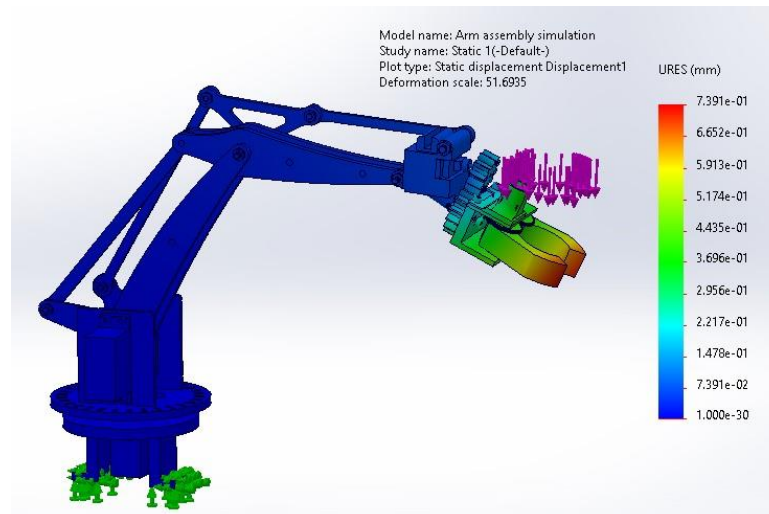


Figure 4.8: Displacement plot of extended robotic arm

Figure 4.9 displays the strain plot of the robotic arm. The contact between the motor used to power the pouring process and the gear connected to it has the greatest deviation from the initial length, which has a value of  $1.505 \times 10^{-3}$  mm/mm. This is due to the motor connection required to support the weight of the gripper support.

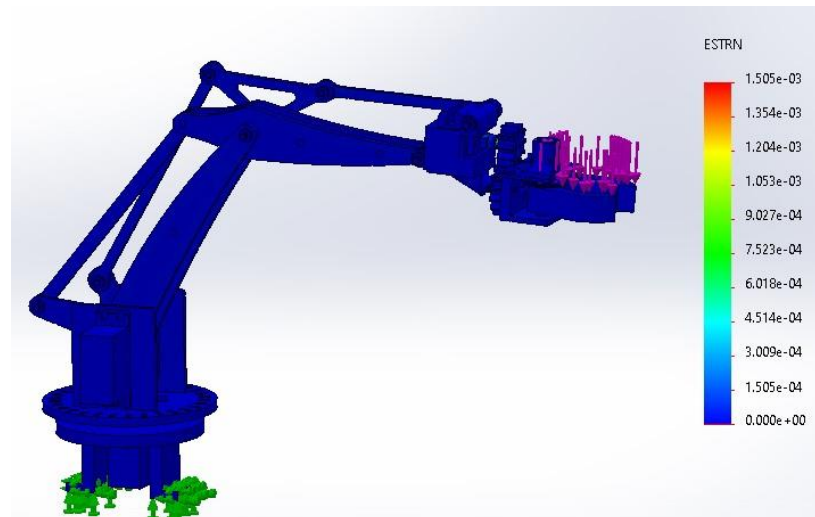


Figure 4.9: Strain plot of extended robotic arm

### 4.3 Centre of mass: Toppling Analysis

In this section, the results obtained from Chapter 3.5 will be shown. The identification of the centre of mass, the calculation of the theoretical topple angle and the identification of the experimental topple angle under four different scenarios will then be discussed.

#### 4.3.1 Centre of mass

Solidworks was used to identify the centre of mass for eight different situations. Figure 4.10 displays the centre of mass measurement in the x, y, and z directions, and Table 4.1 shows the centre of mass obtained from Solidworks.

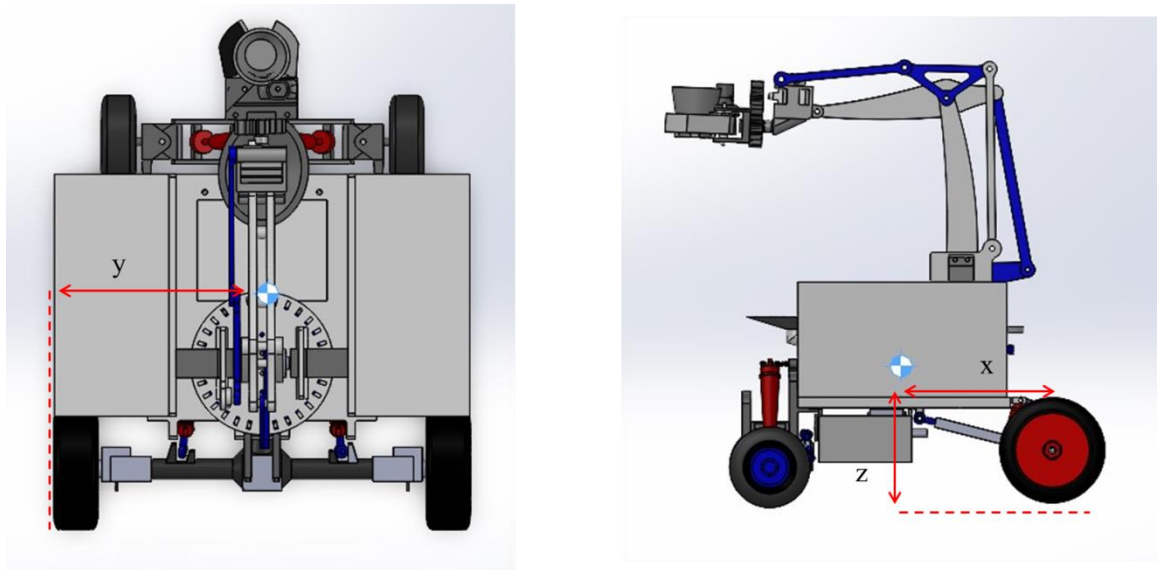


Figure 4.10: Measurement of centre of mass in x, y and z direction

Table 4.1: Centre of mass of robot prototype for eight situations

Scenarios	Arm	Tank	X (mm)	Y (mm)	Z (mm)
1	Retracted	Empty	136.03	110.46	122.13
2		Full	136.55	110.97	122.61
3	Extended	Empty	142.25	105.39	122.02
4		Full	142.71	105.86	122.43
5	Retracted	Empty	124.05	110.03	109.92
6		Full	124.56	110.47	110.34
7	Extended	Empty	124.24	104.12	99.82
8		Full	124.72	104.63	100.21

The robot prototype's centre of mass, as determined from Table 4.1, is within its four wheels in all eight situations, demonstrating that the robot prototype won't topple over while travelling and operating.

### 4.3.2 Topple Angle

Formulas in Chapter 3.5.2 were used to compute the topple angles for eight situations, and the results are shown in Table 4.2.

Table 4.2: Theoretical topple angle for eight scenarios

Scenarios	Arm	Tank	Topple Angle (°)			
			Front	Rear	Left	Right
1	Retracted	Empty	43.22	47.87	50.92	47.02
2		Full	43.22	47.85	50.90	46.99
3	Extended	Empty	42.87	49.18	53.47	46.08
4		Full	42.87	49.15	53.43	46.06
5	Retracted	Empty	46.20	44.97	48.43	44.23
6		Full	46.23	44.97	48.43	44.25
7	Extended	Empty	45.04	43.79	50.04	45.63
8		Full	45.03	43.76	50.01	45.60

$$\text{Percentage error (\%)} = \frac{|\text{theoretical angle} - \text{experimental angle}|}{\text{experimental angle}} \times 100\% \quad (4.1)$$

Table 4.3: Theoretical and Experimental topple angle and percentage errors

Situation		Topple Angle (°)			
		Front	Rear	Left	Right
1. Retracted and Empty	Theoretical	43.22°	47.87°	50.92°	47.02°
	Experimental	41°	41°	46°	41°
	% error	5.41%	16.76%	10.70%	14.68%
2. Extended and Empty	Theoretical	42.87°	49.18°	53.47°	46.08°
	Experimental	37°	41°	46°	41°
	% error	15.86%	19.95%	16.24%	12.39%
3. Retracted and Empty	Theoretical	46.20°	44.97°	48.43°	44.23°
	Experimental	41°	41°	46°	41°
	% error	12.68%	9.68%	5.28%	7.88%
4. Extended	Theoretical	45.04°	43.79°	50.04°	45.63°

and Empty	Experimental	41°	41°	46°	41°
	% error	9.85%	6.80%	8.78%	11.29%

According to the results in Table 4.3, the percentage error has a range of 5.28 % to 19.95 %. It is also observed that the theoretical topple angle is greater than the experimental topple angle. The position of the centre of mass of the prototype in Solidworks will be different with real life situation as the minor parts are not involved in determining the centre of mass. During the experiment, other components such as wire connections and fasteners are included, which leads to a change in the centre of mass. The robot prototype can climb an incline of not less than 37 ° before it topples, and this incline is indeed sufficient for it to navigate through a rubber plantation.

#### **4.4 Prototype test run**

The functional test findings will be addressed in the following section. Two functional tests will be performed; the first is to determine the cycle time of the robot prototype for completing a single cycle of latex cup collection, and the second will evaluate the capability of the manipulation system to collect latex cups that are positioned at different elevations.

##### **4.4.1 Functional test**

The water bottle that serves as the rubber tree is situated 200 mm to the left of the prototype. A distance of 200 mm is suitable for the prototype to collect the latex cup, as there is a length limit for the robotic arm to extend. Figure 4.11 shows the cycle procedure of the robot prototype for collecting the latex cup in a single cycle. The steps of the prototype for collecting the latex cup and the cycle time are shown in Table 4.4. The total cycle time for the prototype to collect the latex cup is

approximately 60 seconds. The cycle will be repeated when the prototype approaches the next water bottle.

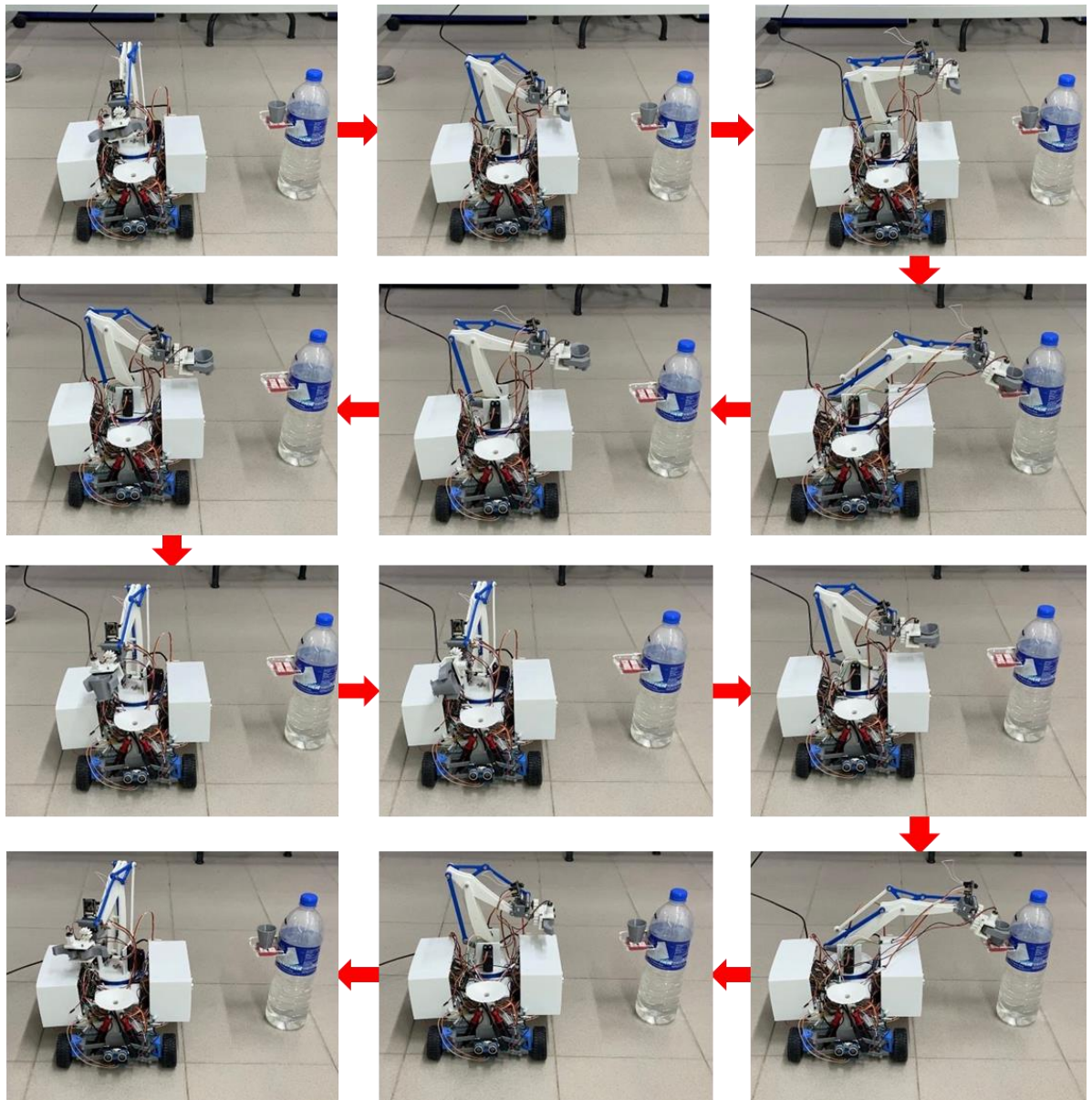


Figure 4.11: Procedure of the prototype to collect latex cup for single cycle

Table 4.4: Steps and cycle time

Steps	Action	Time (seconds)
1	Prototype detected the water bottle	1
2	Robotic arm rotate towards the water bottle	2
3	Adjust position of the arm	2
4	Stop	2

5	Arm extends	3
6	Stop	1
7	Gripper closes	2
8	Stop	1
9	Arm retracts	3
10	Stop	2
11	Adjust position of the arm	2
12	Stop	2
13	Rotate arm towards the latex tank	3
14	Gripper rotates clockwise	1.5
15	Stop	4
16	Gripper rotates anticlockwise	1.5
17	Stop	5
18	Robotic arm rotate towards the water bottle	2
19	Adjust position of the arm	2
20	Stop	1
21	Arm extends	3
22	Stop	1
23	Gripper opens	2
24	Stop	1
25	Arm retracts	3
26	Stop	1
27	Adjust position of the arm	2
28	Stop	2
29	Rotate arm towards the latex tank	2
<b>Total cycle time</b>		<b>60</b>

#### 4.4.2 Manipulator test

The latex cups are positioned at various heights of 190 mm, 150 mm and 90 mm respectively, on three different water bottles. The location of the latex cups was pre-

set in the control software system so that the robotic arm would be able to approach the latex cups and collect them. The process of robotic arm of the robot prototype collects latex cups positioned at 190 mm, 150 mm and 90 mm are illustrated in Figure 4.12, Figure 4.13 and Figure 4.14 respectively.

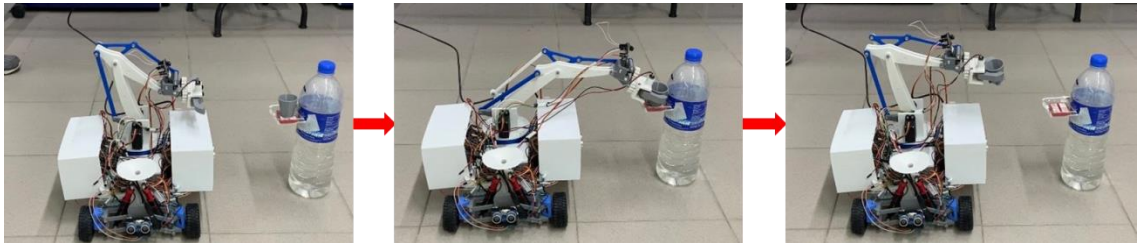


Figure 4.12: Robot collects latex cup positioned at 190 mm height

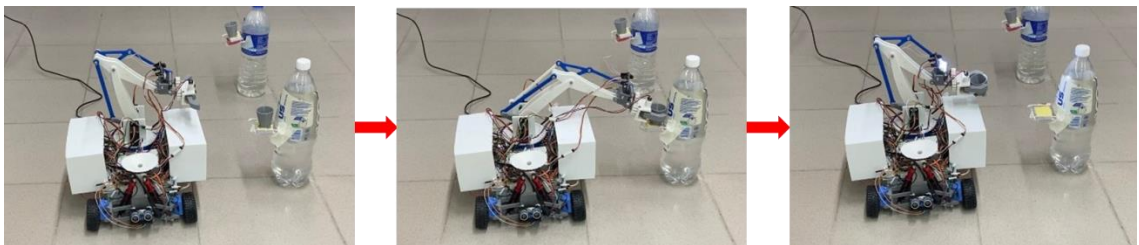


Figure 4.13: Robot collects latex cup positioned at 150 mm height

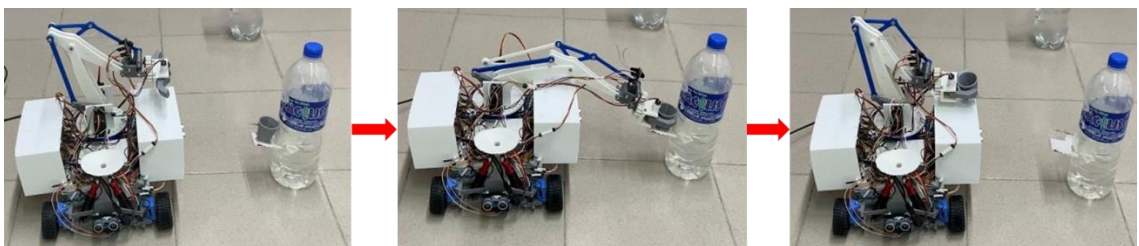


Figure 4.14: Robot collects latex cup positioned at 90 mm height

#### 4.5 Mobility Test

In this section, a mobility test experiment will be conducted to compare with the results obtained from the Solidworks motion study analysis. The results obtained are pitch, yaw and roll of the prototype when travelling across obstacles. Figure 4.15 shows the yaw, pitch, and roll rotation of the robot prototype in Solidworks. Roll

revolves around the x-axis of the body in relation to the centre of mass, whereas pitch and yaw are rotations about the body's y and z axes, respectively.

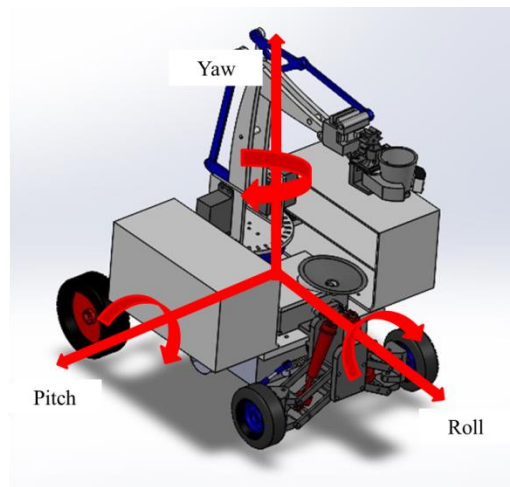


Figure 4.15: Yaw, pitch and roll of the robot prototype

#### 4.5.1 Motion Study

Solidworks was used to simulate the motion studies of the robot prototype and to calculate the angles of yaw, pitch, and roll. Figure 4.16 shows the combined graph of pitch, yaw and roll angles when travelling across the barriers. On the X, Y, and Z axes, a positive result denotes rotation along the axis in a clockwise direction, whereas a negative result denotes rotation along the axis in an anti-clockwise direction.

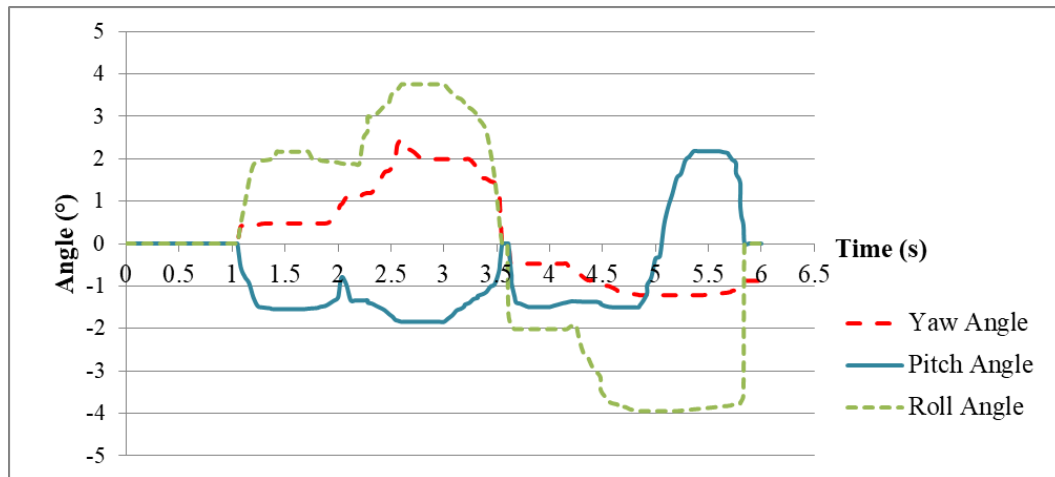


Figure 4.16: Motion study: Yaw, Pitch, and Roll angle ( $^{\circ}$ ) vs. time (s) graph

According to the graph obtained from the motion study, it is observed that the yaw angle increases when passing the barriers. When the robot prototype travelled across the left barriers, the front wheel tilted to the left, which gave a positive value of around  $2.5^{\circ}$  as the yaw angle rotated clockwise. When the robot prototype travels across the right barriers, the front wheel tilts  $-1.2^{\circ}$  to the right as the yaw angle rotates counter-clockwise. The cause of the increase change in direction of yaw angle may be slippage between the wheels and the barriers.

Next, the pitch angles obtained from the motion study are around  $-1.9^{\circ}$  when the front wheels travel across the barriers and around  $2.2^{\circ}$  when the rear wheels travel across the barriers. The front wheels have a smaller pitch angle compared to the rear wheels when moving across the barriers as the spring system at the front wheel has a higher stiffness, which causes the compression of the spring to be smaller.

Lastly, the roll angle experienced the biggest difference when the robot prototype crossed the barriers. The front wheels roll at an angle of around  $2^{\circ}$  and the rear wheels roll at an angle of around  $4^{\circ}$  when crossing either side of the barriers. This is also due to the fact that the front wheel has a higher stiffness, which causes the compression of the spring to be smaller.

### 4.5.2 Mobility Test Run

The barriers that were used to carry out a real life mobility test run were 3D printed to test the availability of the prototype to travel across the barriers. Figure 4.17 and Figure 4.18 illustrate the side view and front view of the robot prototype travelling across the barriers on the left and right sides, respectively. Referring to Figure 4.17, the pitch angle of the prototype can be observed and it was observed that the prototype will tilt forwards and backwards when passing across the barriers. The yaw angle and roll angle can be observed in Figure 4.18. The roll angle was obvious when the prototype travelled across the barriers. The prototype rotates clockwise when travelling across right barriers and anti-clockwise when travelling across left barriers. It is also observed that there is a yaw angle when travelling across the barriers. The robot prototype slid slightly left after travelling across the left barriers. These findings demonstrate that the mobility test was validated.

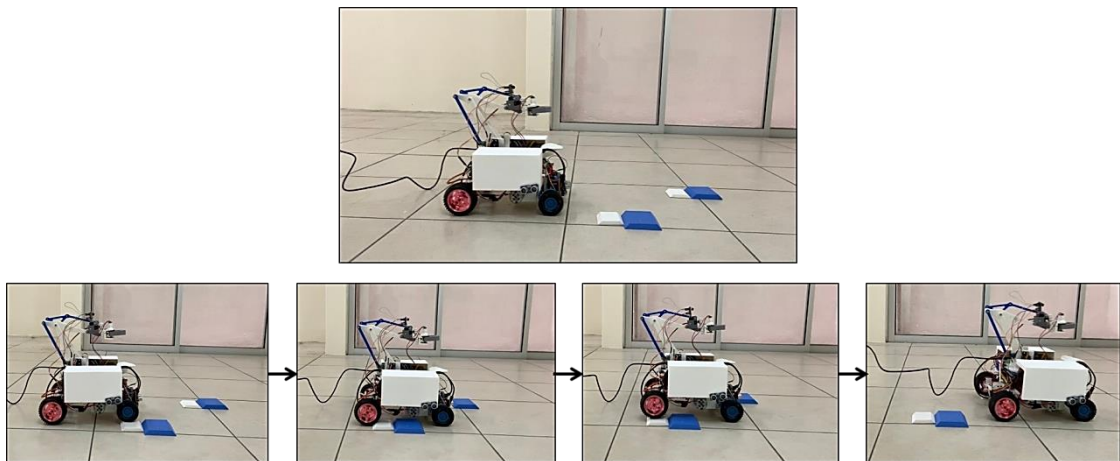


Figure 4.17: Side view of robot prototype travel across left and right barriers

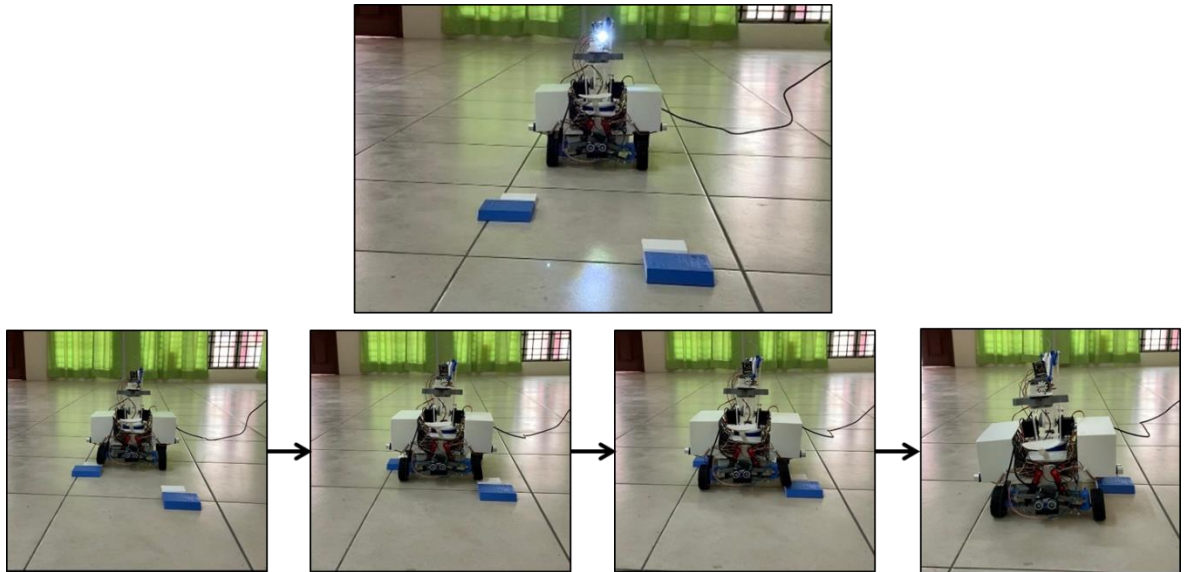


Figure 4.18: Front view of robot prototype travel across left and right barriers

#### 4.6 Comparison with Previous Versions of Robot Prototype

Table 4.5: Comparison of Previous Versions of Robot Prototype with Current Version

	Version 1	Version 2	Version 3 (Current version)
Transmission System	Direct Drive	Differential Drive	Differential Drive
Number of Wheels	2 front wheels, 1 rear wheel	2 front wheels, 2 rear wheels	2 front wheels, 2 rear wheels
Suspension System	-	Double wishbone + spring	Double wishbone + spring
Steering System	-	Ackermann	Ackermann
Manipulator (Degree of Freedom)	3	4	5
End-effector	Gripper	Gripper	Gripper
Cycle time	-	107 seconds	60 seconds
Percentage error of topple angle	42%	24%	20%

Table 4.5 shows the comparison of previous versions of latex cup collector robot prototype with current version. The first version of robot prototype was designed with 3 DoF motor-driven manipulator, direct drive power transmission and does not equipped with suspension system and steering system. The 3 DoF robotic arms have caused the robot prototype not able to collect latex cups located at various heights.

Besides, the prototype may not be able to navigate on unstructured terrain and perform turning due to lack of suspension and steering system. The second version of robot prototype was designed with 4 DoF motor driven manipulator, differential drive power transmission, double wishbone and spring suspension and Ackermann steering. The robot prototype developed is able to collect latex cups at different heights and overcome the obstacles when travelling across uneven surfaces. The third version of the robot prototype is designed with 5 DoF motor driven manipulator, differential drive power transmission, double wishbone and spring suspension, Ackermann steering and equipped with encoder sensor to improve accuracy of angle of rotation of motor. In this project, a robot prototype with 5 DoF of robotic arm will be designed and developed by improving on the previous design. By comparing the third version and previous version, the cycle time to collect latex cups has decreased from 107 seconds to 60 seconds. This is due to the increase of Degree of Freedom (DoF) of the robotic arm. The process has eliminated the turning process for the robot prototype to approach to the “rubber tree” to collect the latex cups. Besides, the percentage of the topple angle has also reduced to around 20% for the third version of robot prototype.

## CHAPTER 5

### CONCLUSION AND RECOMMENDATIONS

#### 5.1 Conclusion

In a nutshell, the project has succeeded in achieving its objectives. The robot prototype designed contains a mobile platform equipped with a motor-driven Five Degree of Freedom (DoF) manipulator arm, Ackermann steering, double wishbone suspension, rear-wheel drive and a latex storage tank to store the latex collected from the trees. The robot prototype has gone through simulations by utilising Solidworks's Finite Element Analysis (FEA) and Motion Study Analysis to validate the results in real world experiments. Besides, the robot prototype has undergone real life testing to determine its stability, including a static test and a balance test. Other than that, the robot prototype has also performed mobility test and test runs to validate its control system. Mobility and performance tests were carried out to also ensure the suitability of the motors chosen for the robot prototype to navigate. The robot prototype is able to collect latex cups that are positioned at various elevations. The results obtained demonstrated that the prototype design is workable and capable of autonomously performing fundamental tasks on the varying topography of the rubber plantation.

#### 5.2 Recommendations

During the design process and test run of the robot prototype, several issues arose that prompted recommendations for improving the existing design for future

development. The issue that required improvement was the robot's inability to navigate in a straight line, which was caused by the differential drive transmission. The wheels were not rotating at the same speed, causing the robot to lean to one side at a lower speed, preventing it from moving straight. Additionally, the motor that drove the movement of the robot was irregularly shaped, causing uneven weight distribution, which also led to the robot leaning towards the heavier side, making it difficult to move straight. To address these issues, it is recommended to convert from a differential drive transmission to a direct drive transmission, which would allow each wheel on each side to have one motor to control, resolving the uneven weight distribution of the motor. Besides, the rear-wheel drive could be changed to all-wheel drive to increase the speed of the robot prototype so that it can travel faster and perform tasks in a shorter time. The Ackermann steering could also change to skid steering to reduce the amount of time it takes to rotate the steering of the wheels to perform the turning process.

## REFERENCES

- Anjum, S., Kamal, N., Khan, U.S., Iqbal, J., Izhar, U., Rasheed, N. and Khan, M.A., 2012. *Design of non-conventional chain drive mechanism for a mini robot*. International Conference of Robotics and Artificial Intelligence, pp. 103-107. IEEE. [e-journal] Available at: <<https://doi.org/10.1109/ICRAI.2012.6413403>> [Accessed 19 August 2022]
- Bechar, A., Vigneault, C., 2016. *Agricultural robots for field operations: Concepts and components*. Science Direct. [e-journal] Available at: <<https://www.sciencedirect.com/science/article/pii/S1537511015301914>> [Accessed 19 August 2022]
- Ben-Ari, M., Mondada, F., 2018. *Robots and Their Applications*. In: *Elements of Robotics*. Springer, Cham. pp 1-20. [e-journal] Available at: <[https://doi.org/10.1007/978-3-319-62533-1\\_1](https://doi.org/10.1007/978-3-319-62533-1_1)> [Accessed 14 August 2022]
- Borneopost., 2019. 'Not many young people involved in agriculture'. [online] Available at: <<https://www.theborneopost.com/2019/08/28/not-many-young-people-involved-in-agriculture/>> [Accessed 15 August 2022]
- Bruzzone, L. and Quaglia, G., 2012. *Review article: locomotion systems for ground mobile robots in unstructured environments*, Mech. Sci., 3, pp. 49–62, [e-journal] Available at: <<https://doi.org/10.5194/ms-3-49-2012> > [Accessed 19 August 2022]
- Bruzzone, L., Nodehi, S. E., & Fanghella, P., 2022. *Tracked Locomotion Systems for Ground Mobile Robots: A Review*. Machines, 10(8), 648. MDPI AG. [e-journal] Available at: <<http://dx.doi.org/10.3390/machines10080648>> [Accessed 19 August 2022]
- Carlo, F., 2018. EEZYbotARM MK2. EEZYrobots [online]. Available at: <[http://www.eezyrobots.it/eba\\_mk2.html#](http://www.eezyrobots.it/eba_mk2.html#)> [Accessed 24 August 2022]
- Claver, J., 2022. *Why the overall adoption rate of agricultural robots is still low*. Future Farming. [online] Available at: <<https://www.futurefarming.com/tech-in-focus/field-robots/why-the-overall-adoption-rate-of-agricultural-robots-is-still-low/>> [Accessed 18 August 2022]
- Costanzo, A.T.D., 2021. *Estimation and Sensor Fusion techniques on an autonomous vehicle* [e-journal] Available at: <<https://webthesis.biblio.polito.it/18269/1/tesi.pdf>> [Accessed 18 January 2023]

- Doi, M.A.C., Yusuff, R.M. and Leman, Z., 2014. *A Preliminary Study of Prevalence of Musculoskeletal Disorders among Malaysian Rubber Tappers*. Academia. [e-journal] Available at: <[https://scholar.google.com/scholar?hl=en&as\\_sdt=0%2C5&q=A+preliminary+study+of+prevalence+of+musculoskeletal+disorders+among+Malaysian+Rubber+Tappers&btnG=](https://scholar.google.com/scholar?hl=en&as_sdt=0%2C5&q=A+preliminary+study+of+prevalence+of+musculoskeletal+disorders+among+Malaysian+Rubber+Tappers&btnG=)> [Accessed 15 August 2022]
- Dublin., 2020. *South East Asia Rubber Market Analysis and Forecasts to 2023*. Globe Newswire. [online] Available at: <<https://www.globenewswire.com/news-release/2020/11/09/2122683/28124/en/South-East-Asia-Rubber-Market-Analysis-and-Forecasts-to-2023.html>> [Accessed 14 August 2022]
- Fauroux, J. C., & Bouzgarrou, B. C., 2012. *Dynamic obstacle-crossing of a wheeled rover with double-wishbone suspension*. In *Field Robotics* (pp. 642-649). [e-journal] Available at: <[https://doi.org/10.1142/9789814374286\\_0075](https://doi.org/10.1142/9789814374286_0075)> [Accessed 20 August 2022]
- Fernandez, B.; Herrera, P. J.; Cerrada, J. A., 2018. *Robust digital control for autonomous skid-steered agricultural robots*. Science Direct. *Computers and Electronics in Agriculture*, 15, 94–101. [e-journal] Available at: <[doi:10.1016/j.compag.2018.07.038](https://doi.org/10.1016/j.compag.2018.07.038)> [Accessed 19 August 2022]
- Fue, K.G., Porter, W.M., Barnes, E.M. and Rains, G.C., 2020. *An extensive review of mobile agricultural robotics for field operations: focus on cotton harvesting*. *AgriEngineering*, 2(1), [e-journal] pp.150-174. <<https://doi.org/10.3390/agriengineering2010010>> [Accessed 19 August 2022]
- Ginger, S., 2021. *ZSL report reveals COVID-19 impact on natural rubber producers*. [online] Available at: <<https://www.spott.org/news/zsl-report-reveals-covid-19-impact-on-natural-rubber-producers/>> [Accessed 15 August 2022]
- Goms, G., 2011. *The Role of Springs in Suspension Systems* [online] Available at: <<https://www.tirereview.com/the-role-of-springs-in-suspension-systems/>> [Accessed 20 August 2022]
- Gonzalez, C., 2015. *An overview on the differences between powered actuators and their benefits*. *MachineDesign* [online] Available at: <<https://www.machinedesign.com/mechanical-motion-systems/linear-motion/article/21832047/whats-the-difference-between-pneumatic-hydraulic-and-electrical-actuators>> [Accessed 20 August 2022]
- Hoogewijs, D., 2020. *Research and design of an autonomous and collaborative guided vehicle prototype, to be applied in indoor and outdoor environments and different types of floor*. [online]. Available at: <<https://repositorio.ufscar.br/handle/ufscar/13994>> [Accessed 19 August 2022]
- Hrbáček, J., Ripel, T. and Krejsa, J., 2010. *Ackermann mobile robot chassis with independent rear wheel drives*. *Proceedings of 14th International Power Electronics and Motion Control Conference EPE-PEMC 2010*, Ohrid, Macedonia,

6-8. [e-journal] Available at: <<https://doi.org/10.1109/EPEPEMC.2010.5606853>> [Accessed 19 August 2022]

Inc., 2020. *Robotics*. [online] Available at: <<https://www.inc.com/encyclopedia/robotics.html>> [Accessed 13 August 2022]

Kang, S. J., Wong, C.S., Lim, C.H., Tan, Y. C., 2021. *Design and development of an automated robot for collecting latex cups in rubber plantation*. IOP Science. [e-article] Available at: <<https://iopscience.iop.org/article/10.1088/1755-1315/945/1/012015/pdf>> [Accessed 1 September 2022]

Khor, X. B., 2022. Design and Development of a Controller for Latex Cups Collector Robot [Bachelor's thesis, Universiti Tunku Abdul Rahman]. Universiti Tunku Abdul Rahman.

Khurmi, R.S., Gupta, J.K., 2005. A textbook of Machine Design pp. 759-775. [e-book] Available at: <[https://books.google.com.my/books?id=6FZ9UvDgBoMC&printsec=frontcover&source=gbs\\_ge\\_summary\\_r&cad=0#v=onepage&q&f=false](https://books.google.com.my/books?id=6FZ9UvDgBoMC&printsec=frontcover&source=gbs_ge_summary_r&cad=0#v=onepage&q&f=false)> [Accessed 12 January 2023]

Liné, 2020. *Latex vs Rubber: is it the same thing?* [online] Available at: <<https://ecoworldonline.com/latex-vs-rubber-is-it-the-same-thing/>> [Accessed 18 August 2022]

Malaysian Rubber Council., 2021. *World Rubber Production, Consumption and Trade*. [online] Available at: <[https://www.myrubbercouncil.com/industry/world\\_production.php](https://www.myrubbercouncil.com/industry/world_production.php)> [Accessed 14 August 2022]

Matweb., 2020. Overview of materials for Polylactic Acid (PLA) Biopolymer [Online]. Available at: <<http://www.matweb.com/search/DataSheet.aspx?MatGUID=ab96a4c0655c4018a8785ac4031b9278>> [Accessed 24 August 2022]

Moravec, H. P., 2022. *Robot*. Encyclopedia Britannica. [online] Available at: <<https://www.britannica.com/technology/robot-technology>> [Accessed 13 August 2022]

Nakajima, S., 2011. *RT-Mover: a rough terrain mobile robot with a simple leg-wheel hybrid mechanism*. The International Journal of Robotics Research, 30(13), pp.1609–1626. [e-journal] Available at: <<https://doi.org/10.1177%2F0278364911405697>> [Accessed 19 August 2022]

Neal, A.J., n.d. Tips for Selecting DC Motors For Your Mobile Robot. Servo Magazine blog, [blog] Available at: <[https://www.servomagazine.com/magazine/article/tips\\_for\\_selecting\\_dc\\_motors\\_for\\_your\\_mobile\\_robot#](https://www.servomagazine.com/magazine/article/tips_for_selecting_dc_motors_for_your_mobile_robot#)> [Accessed 25 August 2022]

- Oliveira, L.F., Moreira, A.P. and Silva, M.F., 2021. Advances in agriculture robotics: A state-of-the-art review and challenges ahead. *Robotics*, 10(2), pp.52. [e-journal] <https://doi.org/10.3390/robotics10020052> [Accessed 15 August 2022]
- OnAllCylinders, 2017. *What is a Wishbone Suspension and How Does it Work?* OnAllCylinders. [online] Available at: < <https://www.onallcylinders.com/2017/11/23/wishbone-suspension-work/> > [Accessed 20 August 2022]
- ROBOTIC INDUSTRIES ASSOCIATION (RIA), 2017. *Robots' benefits in the agricultural industry*. *Control Engineering*. [online] Available at: < <https://www.controleng.com/articles/robots-benefits-in-the-agricultural-industry/> > [Accessed 14 August 2022]
- Roh, S.G., Lim, B., Moon, H., Lee, J.S., Park, J.H., Koo, J.C. and Choi, H.R., 2013. *Flexible suspension mechanism for stable driving of a differential drive mobile robot*. *IEEE/RSJ International Conference on Intelligent Robots and Systems*, p.5518-5523. [e-journal] Available at: <<https://doi.org/10.1109/IROS.2013.6697156>> [Accessed 20 August 2022]
- SGrobot, n.d. *A58SW-555 12V Worm Gear High Speed & Torque DC Motor \ Shopee Malaysia* [online] Available at: < <https://shopee.com.my/A58SW-555-12V-Worm-Gear-High-Speed-Torque-DC-Motor-i.33287405.790990474> > [Accessed 19 January 2023]
- Skill-Lync, 2022. *Ackerman's Principle of Steering: Working & Applications*. Skill-Lync. [online] Available at: <<https://skill-lync.com/blogs/ackermans-principle-of-steering-working-and-applications>> [Accessed 19 August 2022]
- Sundar, S., Sudarsanan, T. and Krishnan, R., 2018. *Review of Design and Fabrication of four-wheel Steering system*. *International Journal of Recent Trends in Engineering & Research (IJRTER)*, 4(10), pp.1034-1049. [e-journal] Available at: <[https://www.researchgate.net/publication/330134210\\_Review\\_of\\_Design\\_and\\_Fabrication\\_of\\_four\\_wheel\\_Steering\\_system](https://www.researchgate.net/publication/330134210_Review_of_Design_and_Fabrication_of_four_wheel_Steering_system)> [Accessed 20 August 2022]
- Technology Robotix Society, 2019. *Rocker Bogie Mechanism*. *MANUAL ROBOTICS*. [online] Available at: < <https://medium.com/manual-robotics/rocker-bogie-mechanism-9e75c84a5853> > [Accessed 20 August 2022]
- Tedeschi, F.; Carbone, G., 2014. *Design Issues for Hexapod Walking Robots*. *Robotics*, 3(2), 181-206. MDPI AG. [e-journal] Available at: <<https://doi.org/10.3390/robotics3020181>> [Accessed 19 August 2022]
- Townsend, B., 2002. *Static and kinetic friction*. [online] Available at: < [http://ffden-2.phys.uaf.edu/211\\_fall2002.web.dir/ben\\_townsend/StaticandKineticFriction.htm](http://ffden-2.phys.uaf.edu/211_fall2002.web.dir/ben_townsend/StaticandKineticFriction.htm) > [Accessed 25 August 2022]

- Universal Robots, 2022. *TYPES OF GRIPPERS USED IN MANUFACTURING* [blog] Available at: <<https://www.universal-robots.com/blog/types-of-grippers-used-in-manufacturing/>> [Accessed 24 August 2022]
- Uribe-Holguin, N. C., 2020. *The benefits of robots in agriculture*. LinkedIn. [online] Available at: <<https://www.linkedin.com/pulse/benefits-robots-agriculture-nicolas-chevillotte-uribe-holguin>> [Accessed 14 August 2022]
- Wang, S., Zhou, H., Zhang, C., Ge, L., 2022. *Design, development and evaluation of latex harvesting robot based on flexible Toggle*. Science Direct. [e-journal] Available at: <<https://www.sciencedirect.com/science/article/pii/S0921889021001913#b9>> [Accessed 15 August 2022]
- Xu, Q., Li, H., Wang, Q., & Wang, C., 2021. *Wheel Deflection Control of Agricultural Vehicles with Four-Wheel Independent Omnidirectional Steering*. Actuators, 10(12), 334. MDPI AG. [e-journal] Available at: <<http://dx.doi.org/10.3390/act10120334>> [Accessed 19 August 2022]
- Zhang, F., Wang, Y., Teng, S., Zheng, L., Wang, J. and Chen, Z., 2019. *Development of agricultural bionic four-legged robot: Effect of head movement adjustment on the stability of goats*. International Journal of Agricultural and Biological Engineering, [online] Available at: <<http://www.ijabe.org/index.php/ijabe/article/view/4287> > [Accessed 19 August 2022]
- Zhou, H., Zhang, S., Zhang, C., Zhang, J., 2021. *Design, development, and field evaluation of a rubber tapping robot*. Research Gate. [e-journal] Available at: <[https://www.researchgate.net/publication/354772211\\_Design\\_development\\_and\\_field\\_evaluation\\_of\\_a\\_rubber\\_tapping\\_robot](https://www.researchgate.net/publication/354772211_Design_development_and_field_evaluation_of_a_rubber_tapping_robot) > [Accessed 15 August 2022]
- Gossett, S., n.d. 16 Agricultural Robots and Farm Robots You Should Know. BuiltIn [online] Available at: <<https://builtin.com/robotics/farming-agricultural-robots>> [Accessed 15 August 2022]
- Sacrewell Farm., 2017. *Why do tractors have smaller wheels at the front and larger wheels at the back?* [online] Available at: <<https://www.sacrewell.org.uk/news/why-do-tractors-have-smaller-wheels-at-the-front-and-larger-wheels-at-the-back/>> [Accessed 14 Aug. 2021]
- Youtube, 2017. *SolidWorks Tutorial # 310: Robotic arm (layout design, mate controller)* [online] Available at: <<https://www.youtube.com/watch?v=pVY0Wt4LXUs&t=1s>> [Accessed 10 August 2022]
- Sahuri, Ardika, R., Tistama, R. and Oktavia, F., 2021. A review : The development of double row spacing to improve land productivity and income of rubber smallholders. [e-journal] Available at: <<https://doi.org/10.1051/e3sconf/202130503002>> [Accessed 9 January 2023]